

2009-04

# Record of Cenozoic sedimentation from the Amanos Mountains, Southern Turkey: Implications for the inception and evolution of the ArabiaEurasia continental collision

Boulton, SJ

<http://hdl.handle.net/10026.1/3044>

---

10.1016/j.sedgeo.2009.01.008

Sedimentary Geology

Elsevier BV

---

*All content in PEARL is protected by copyright law. Author manuscripts are made available in accordance with publisher policies. Please cite only the published version using the details provided on the item record or document. In the absence of an open licence (e.g. Creative Commons), permissions for further reuse of content should be sought from the publisher or author.*

1 **NOTICE: this is the author's version of a work that was accepted for publication in**  
2 **Sedimentary Geology. Changes resulting from the publishing process, such as peer review,**  
3 **editing, corrections, structural formatting, and other quality control mechanisms may not be**  
4 **reflected in this document. Changes may have been made to this work since it was submitted**  
5 **for publication. A definitive version was subsequently published in Sedimentary Geology, 216,**  
6 **29-47 (2009). doi:10.1016/j.sedgeo.2009.01.008**  
7

8

9 **Record of Cenozoic sedimentation from the Amanos Mountains, Southern Turkey:**  
10 **implications for the inception and evolution of the Arabia-Eurasia continental collision**

11

12 Sarah J. Boulton

13

14 School of Earth, Ocean and Environmental Sciences, University of Plymouth, Drakes Circus,  
15 Plymouth, PL4 8AA, UK.

16 E-mail - sarah.boulton@plymouth.ac.uk; fax: 01752 233117

17

18

19 **Abstract**

20 The sedimentary succession of the southern Amanos Mountains, bordering the eastern margin of the  
21 Karasu Rift in south central Turkey, provides a record of environmental change from the Eocene  
22 (Lutetian) to the Upper Miocene (Tortonian) that charts the final evolution of the northern margin of  
23 the Arabian plate prior to and during continental collision. Eocene shallow-marine carbonates  
24 (Hacıdağı Formation) are interpreted as the youngest unit of the Arabian passive margin succession  
25 deposited on a northwards facing carbonate ramp. Subsequent deformation and uplift took place  
26 during the Oligocene represented by folding of the Eocene and older strata. This is interpreted to be  
27 the result of initial continental collision between Arabia and Eurasia. Unconformably overlying the  
28 Eocene limestone are Lower Miocene conglomerates, sandstones and palaeosols up to 150 m thick  
29 (K1c1 Formation). These were deposited in a range of marginal marine settings consisting of alluvial

30 fan/fan delta facies, flood plain as well as basinal facies. Subsequently, during the Middle Miocene,  
31 local patch reefs developed in restricted areas (Kepez Formation) followed by Upper Miocene  
32 sediments (Gökdere Formation) composed of relatively deep water hemipelagic marl, with clastic  
33 interbeds, which represent a transgression during this period. The Upper Miocene becomes sandier  
34 upwards, this records the regression from the relatively deep water facies to coastal sediments. Water  
35 depth gradually became shallower until during Pliocene time the area became continental in nature.  
36 By the Quaternary rifting had resulted in the development of the Karasu Rift with active alluvial fans  
37 along the margins and braided rivers depositing coarse conglomerates in the axial zone. These  
38 conglomerates are interbedded with basaltic lava flows that resulted from the region extension across  
39 the area. This research shows that initial continental collision occurred in this area after the Lutetian  
40 (40.4 Ma) and before the Aquitanian (23.03 Ma) supporting the hypothesis that the southern  
41 Neotethys Ocean closed during the Late Eocene to Oligocene. This was a time of climatic change  
42 including the onset of southern hemisphere glaciation, in which the closure of the southern Neotethys  
43 may have had played an important role.

44

45 Key words: Neogene, carbonate ramp, alluvial fan, continental collision, Dead Sea Fault, Neotethys,  
46 Eocene-Oligocene boundary.

47 **Cite as:** Boulton, S. J., 2009. Record of Cenozoic sedimentation from the Amanos Mountains,  
48 Southern Turkey: implications for the inception and evolution of the Arabia-Eurasia continental  
49 collision. *Sedimentary Geology*. 216, 29-47. doi:10.1016/j.sedgeo.2009.01.008

50

## 51 **1 Introduction**

52 It is now generally accepted that the geology of southern Turkey records evidence for the  
53 evolution and closure of the Southern Neotethys Ocean and the timing of the collision between

54 Arabia and Anatolia (Sengor and Yilmaz, 1981; Robertson and Dixon, 1984; Yilmaz et al., 1993;  
55 Robertson, 2000; Robertson et al., 2004; Robertson et al., 2006). However, there is still much  
56 debate on when the northward subduction of Arabia beneath Anatolia ceased and when the closure  
57 of the southern Neotethys and subsequent continental collision actually took place (Hall, 1976;  
58 Aktaş and Robertson, 1984; Yilmaz et al., 1993; Beyarslan and Bingöl; 2000). There are three main  
59 alternative theories, with collision occurring either during: 1) the Late Cretaceous (Karig and Kozlu,  
60 1990; Kozlu 1997; Beyarslan and Bingöl, 2000); 2) in the Late Eocene (Vincent et al., 2007; Allen  
61 and Armstrong, 2008) or 3) during the Oligocene to Early Miocene (Aktaş and Robertson, 1984;  
62 Yilmaz et al., 1993; Robertson, 2000; Robertson et al., 2004; Robertson et al., 2006) along a suture  
63 that runs through SE Turkey (Bitlis Suture; Fig. 1) and into Iran (Zagros Suture; Fig. 1).

64 The Tertiary evolution of the northern margin of the southern Neotethys has attracted much  
65 attention (e.g. Hall, 1976; Aktaş and Robertson, 1984; Yilmaz et al., 1993; Beyarslan and Bingöl,  
66 2000; Robertson, 2000; Robertson et al., 2004; Robertson et al., 2006), but there has been less focus  
67 on the coeval evolution of the Arabian margin in the west. Research has been carried out on  
68 Cenozoic sediments found within the Bitlis suture zone. These sediments are thought to have been  
69 deposited within basins assumed to be representative either of a peripheral foreland basin (Şengör  
70 and Yilmaz, 1981; Kelling, 1987) or of small transtensional basins (Karig and Kozlu, 1990; Kozlu,  
71 1997). Additionally, there is some work focussing on the evolution and role of Cenozoic basins on  
72 the Arabian platform that are today > 100 km from the suture zone (Hatay Graben, Turkey; Boulton  
73 et al., 2006; Boulton and Robertson, 2007: Nahr El-Kabir half-graben, Syria; Hardenberg and  
74 Robertson, 2007). Conversely, much of the work on the Arabian margin has concentrated on the  
75 Zagros region in Iran and Iraq, 1000s of kilometres to the east (Hessami et al., 2001; Agard et al.,  
76 2005; Vincent et al., 2005) and therefore, may not be representative of regions to the west if  
77 continental collision was diachronous.

78 In this paper, I will present the first modern descriptions and interpretation of the Eocene to  
79 Late Miocene sedimentary sequence from the southern end of the Amanos Mountains, ~ 50 km

80 south of the suture zone (Figs. 1, 2). This study focuses on the area around the towns of Kırıkhan,  
81 Belen and Serinyol in the Hatay Province of southern Turkey where Cenozoic strata outcrop in the  
82 Amanos Mountains due to uplift on the flanks of the Plio-Quaternary Karasu Rift. New  
83 sedimentological and petrological data are presented for these rocks based upon a recent  
84 redefinition of the stratigraphic framework (Boulton et al., 2007). This allows new  
85 palaeoenvironmental interpretations to be made and implications drawn for the palaeogeographic  
86 evolution of the northern Arabian plate margin during the final stages of continental collision and  
87 the subsequent development of a peripheral foreland basin on the Arabian plate.

88

## 89 **2 Geological Framework**

90 The DSFZ system forms the boundary between Arabia and Africa (Fig. 1), accommodating the  
91 difference in motion between the two plates through sinistral strike-slip motion. The DSFZ trends ~  
92 N-S from the Red Sea, in the south, to the junction with the East Anatolian Fault Zone (EAFZ) near  
93 Kahramanmaraş in southern Turkey, in the north. The DSFZ developed, in the south, during the  
94 Middle Miocene (dated as <20 Ma, Lyberis, 1988; 18 Ma, Garfunkel and Ben Avraham, 1996) with  
95 the slip rate calculated as ~7 mmyr<sup>-1</sup> (Garfunkel et al., 1981).

96 The Karasu Rift forms the northernmost segment of the Dead Sea Fault Zone (DSFZ), located  
97 primarily in the Hatay Province of Turkey, trending northwards from the Amik Plain (Fig. 1). To  
98 the south of the Amik Plain, the Gharb Rift forms the southwards continuation of the DSFZ; while  
99 to the east another structure, the Hatay Graben, trends NE-SW to the present Mediterranean coast.  
100 The Karasu Rift can be subdivided into three segments (Rojay et al., 2001); northern, central and  
101 southern. This paper will focus on the western margin of the southern segment of the Karasu Rift  
102 from Kırıkhan in the north to Serinyol in the south.

103 The Karasu Rift is bounded by two main faults the Amanos Fault Zone (AFZ) in the west  
104 and the East Hatay Fault (EHF) in the east (Fig. 1). Slip rate estimates of the AFZ from offset

105 lavas range from  $0.3 \text{ mmyr}^{-1}$  (Arger et al., 2000, based upon data from Çapan et al., 1987), 2 – 15  
 106  $\text{mmyr}^{-1}$  (Rojay et al., 2001), 1 –  $1.6 \text{ mmyr}^{-1}$  (Yurtmen et al., 2002) to  $4 \text{ mmyr}^{-1}$  (Tatar et al., 2004).  
 107 There are few estimates for the slip rates of the EHF, amongst which those of Tatar et al., (2004)  
 108 who derived a figure of  $4 \text{ mmyr}^{-1}$  for the EHF. Although motion on these faults is dominantly  
 109 sinistral strike-slip there is a normal component of motion that has lead to the development of the  
 110 Karasu Rift and, which caused the uplift of the Amanos Mountains to the west of the rift. The  
 111 Amanos Mountains are composed of a core of metamorphosed Precambrian rocks, Palaeozoic  
 112 sediments, ophiolite and Cenozoic sedimentary cover, whereas the rift fill is poorly exposed recent  
 113 alluvium with interbedded lavas (Fig. 2).

114 Pioneering geological research in the study area was undertaken by Dubertret (1939, 1953),  
 115 followed by the first subdivision of the Palaeozoic rocks of the Amanos Mountains by Dean and  
 116 Krummenacher (1961) and of the complete stratigraphic sequence by Atan (1969). Geological  
 117 mapping of the Amanos Mountains as a whole was undertaken by Schwan (1971), Ishmawi (1972),  
 118 Janetzko (1972) and Lahner (1972) but these works generally lacked widespread correlation and  
 119 palaeontological age constraints. The 1980s saw an increased interest in the area by the Turkish  
 120 Petroleum Corporation (detailed list in Dean et al., 1986). Although the majority of this work is still  
 121 unpublished, the work of Guney (1984) presents important micropalaeontological biozonation of  
 122 Cenozoic formations. Piskin et al., (1986) published a new geological map for the Hatay region,  
 123 with a brief synopsis of the sedimentary units based mostly on the earlier work of Atan (1969). In  
 124 the same year, Dean et al., (1986) presented a revised stratigraphic scheme for the Palaeozoic  
 125 sediments of the southern Amanos area (around Kırıkhan), which did not include the Cenozoic  
 126 stratigraphy. Further geological mapping in the Kırıkhan and Belen areas was undertaken by Kop  
 127 (1996) and Dokumaci (1997).

128 It is evident that the sedimentary cover has only received rudimentary attention, in  
 129 comparison to the detailed analysis and interpretation of the Upper Cretaceous ophiolite (e.g.,  
 130 Çogulu, 1974; Delaloye et al., 1980; Piskin et al., 1986), the structural geology of the Karasu Rift

131 (e.g., Saroglu et al., 1992; Rojay et al., 2001; Westaway and Arger, 2001; Adiyaman and  
132 Chorowicz, 2002; Over et al., 2002; Yurtmen et al., 2002; Westaway, 2003; Tatar et al., 2004;  
133 Akyuz et al., 2006) and the nature of the Karasu basalts (Çapan et al., 1987; Parlak et al., 1998;  
134 Rojay et al., 2001; Yurtmen et al., 2002; Tatar et al., 2004).

135

### 136 **3 Cenozoic sediments of the Karasu Rift**

137 The Cenozoic sediments of the Southern Karasu Rift (Table 1) occur predominantly around the  
138 towns of Kırıkhan, on the western edge of the Karasu Rift, and Belen in the Amanos Mountains  
139 (Fig. 2). The strata range from Eocene to Late Miocene in age, the Eocene strata are folded and  
140 faulted (Boulton and Robertson, 2008) and unconformably overlain by relatively undeformed  
141 Neogene sedimentary rocks. This sedimentary cover overlies the Hatay/Kızıldağ Ophiolite that was  
142 emplaced southwards during the Maastrichtian (Robertson, 2002). A smaller outcrop of Cenozoic-  
143 aged sediment is preserved on the edge of the Amik Plain around the town of Serinyol, to the north  
144 of Antakya and southwest of Kırıkhan. This area lies in the southernmost part of the Karasu Rift  
145 within a re-entrant of the ophiolite. A sequence of Palaeocene-Eocene to Upper Miocene  
146 sedimentary rocks is exposed in this small area (Fig. 3). In this section sedimentary descriptions and  
147 interpretations of the Cenozoic units are given, which are then used to build a model of  
148 palaeogeographic change in the study area allowing comparisons to other areas and an evaluation of  
149 major tectonic events.

150

#### 151 **3.1 Eocene limestone - Hacıdağı Formation.**

152 There are large exposures of Eocene limestone along the Belen and Kırıkhan roads to Antakya. The  
153 limestone (Hacıdağı Formation) varies from fine-grained wackestone and packstone to rudstone.  
154 Bedding is thin (0.1-0.2 m thick) with sharp bases and tops and often normally graded, bases of  
155 some beds are erosional and many are laterally discontinuous. Additionally, bedding is disrupted in

156 places where slumping has occurred or was incipient (Figs. 4a, b). Data from fold hinges and  
157 bedding in slumped horizons indicates a general  $\sim 000^\circ - 020^\circ$  for the down-slope direction (Fig. 5).  
158 Planar lamination is common, and there is abundant bioturbation, where burrows can be seen to cut  
159 and disrupt the laminations in some beds. There are numerous large benthic foraminifera, often  
160 concentrated in lags at the bases of the beds. Planktic foraminifera are also reported from these  
161 limestones such as *Globorotalia velascoensis* (Cushman), but benthic species are the most diverse  
162 (*Nummulites* sp., *Discocyclusina* sp., *Orbitolites* sp., *Alveolina* sp., *Assilina* sp. (Atan, 1969)) dating  
163 the formation to the Lutetian (Boulton et al., 2007). Chert is common, forming dark grey to black,  
164 elongated nodules parallel to the bedding planes. Occasionally there are horizons of angular- to  
165 well-rounded clasts, composed of limestone and serpentinite. Overlying these thinly bedded  
166 limestones is a laterally extensive bed,  $\sim 10$  m thick, that has an erosive base. This is a matrix-  
167 supported conglomerate with sub-rounded clasts of fine-grained, white limestone ( $< 70$  mm) in a  
168 matrix of non-fossiliferous white nummulitic wackestone/floatstone.

169 Along the Belen-Antakya road section, the basal contact between the Hacıdađı Formation  
170 and the underlying ophiolite (sheeted dyke complex) is generally sharp and does not appear to have  
171 any basal conglomerate or other lithological changes associated with it, and is therefore interpreted  
172 as a faulted contact. The upper boundary of the formation can be observed on the main road just  
173 before Belen. The top of the Eocene limestone is eroded and bedding is sub-vertical. Overlying  
174 basal Miocene sediments contain well-rounded clasts of Eocene limestone indicating an erosional  
175 contact.

176 Eocene limestones are also exposed along a riverbed near Serinyol (Fig. 6b). Here the  
177 formation (Fig. 3) directly overlies the eroded upper surface of the ophiolite, along a disconformity.  
178 The base of the sequence is composed of hard white limestone (wackestone-packstone) containing  
179 large benthic foraminifera (*Nummulites*, *Discocyclusina*) and common chert nodules. Within this  
180 basal limestone there is a large, laterally discontinuous, conglomerate horizon (Fig. 4c), the base of  
181 which is irregular and cuts down to the top of the ophiolite in the north. This conglomerate is



182 poorly sorted and clast supported, composed entirely of sub-angular to sub-rounded, limestone and  
183 chert clasts (Table 1) up to 0.9 m in size. The matrix is sandy and contains *Amphistegina* sp.,  
184 *Operculina* sp., *Rotalia viennotti*, *Quinqueloculina* sp., *Globigerina* sp., *Miogypsina* sp., *Textularia*  
185 sp., *Lepidocyclina* sp., and unidentifiable foraminifera of the Rotaliina. There are also fragments of  
186 *Lithophyllum*.

187 Above the conglomerate, there is a return to limestone (fine-grained sparite). Bedding is thin  
188 and irregular; the upper surfaces of the beds occasionally exhibit current ripples. Chert nodules are  
189 very common and *Nummulites* and other large benthic foraminifera are occasionally observed in  
190 dense accumulations. Within this sequence there are several clast supported conglomerate horizons;  
191 the clasts are angular to sub-rounded, <0.5 m in size and composed of limestone and chert. There is  
192 also a thick (2.5 m) rudstone bed that has an irregular base that cuts down into the underlying beds.  
193 *Nummulites* and *Discocyclina* exhibit a rough parallel alignment. Additionally, there is a small  
194 change in bedding orientation above and below this bed.

195 A conglomerate horizon is observed near the abandoned village of Kanlidere (Fig. 6a).  
196 Thin-bedded, wackestone with chert nodules is exposed in the valley bottom. The top of the  
197 formation is a 7-10 m thick, clast-supported conglomerate, clasts are sub-angular to sub-rounded  
198 composed of limestone and chert (Table 3), with a maximum clast size of 0.3 m. Although  
199 generally poorly sorted there are horizons within the conglomerate that exhibit better sorting.

### 200 3.1.1 Interpretation

201 The characteristic planar beds, which fine-upwards and exhibit parallel lamination, suggest  
202 that these limestones were deposited from low density turbidity currents consisting of the T<sub>abe</sub>  
203 divisions of the classical Bouma sequence (Bouma, 1962). The T<sub>cd</sub> divisions of the Bouma  
204 sequence are generally absent, suggesting that partial flow separation may have taken place  
205 resulting in incomplete sequences.

206 Some horizons are distorted and broken; these were interpreted as incipient slumps as the  
207 bedding was broken but significant offset in the bedding planes had not occurred (Fig 4a). Other

208 horizons show more obvious evidence of slumping including a spectacular isoclinal fold (Fig. 4b).  
209 The orientation of these structures indicates the presence of a northward-dipping slope (Fig. 5). The  
210 thin-bedded facies are commonly capped by a thick bed of laterally extensive, matrix-supported  
211 conglomerate. The clast size, shape and overall texture suggest the conglomerate was probably lain  
212 down by a powerful a debris flow (Nilsen, 1982).

213 Poorly sorted, clast-supported conglomerates were observed at Serinyol and Kanlidere (Fig.  
214 6). The clast-supported nature suggests deposition was not by a debris-flow process but that it was  
215 deposited from a hyperconcentrated sediment flow. In addition, several conglomerate horizons are  
216 present near Serinyol. The main conglomerate bed cuts out the basal part of the underlying bedded  
217 Eocene limestone and sits directly on top of the underlying ophiolite. It is probable that this  
218 conglomerate represents a channel fill; however, it was not possible to determine the channel  
219 orientation. Foraminifera identified in the matrix indicate derivation from a shelf environment.  
220 Near the top of the sequence there is a widespread but slight angular (1-2°) discordance within the  
221 formation, directly below this there is a thick bed of Nummulitic rudstone with an erosive base; this  
222 may be the result of scouring, possibly following a tectonic event. Only one conglomerate horizon  
223 was observed at Kanlidere. The lenticular nature of these clast-supported conglomerates suggests  
224 that these could be channel-fill deposits or scour fills.

225 The abundance of large benthic foraminifera and low abundance of planktic forms indicates  
226 relatively shallow water depths. The presence of *Nummulites* sp., in particular indicates water  
227 depths of 20 – 75 m (Saller et al., 1993) although reworking to deeper water is likely as the  
228 foraminifera are often found in concentrated lags.

229 Therefore, the biotal evidence combined with evidence for sediment instability and  
230 movement (slumps, turbidites and channel fills) suggests that during the Eocene in this northern  
231 area, carbonates were being deposited on a slope, orientated approximately northwards. The slope  
232 was unstable generating debris flows and turbidity currents and was cut into by large channels that  
233 were in-filled by coarse-grained sediments.

234

**235 3.2 Lower Miocene sandstone and conglomerates - Kıcı Formation.**

236 The base of the Kıcı Formation rests unconformably on the Eocene at the type section near  
237 Kurtisoguksu (K; Fig. 2); as is the case throughout the area as Oligocene sediments are absent. A  
238 thick-bedded, dominantly matrix-supported conglomerate unit, 50-60 m thick, is present at the base  
239 of the section (Fig. 7). Clasts are up to 1 m in size, angular to sub-rounded and composed  
240 dominantly of carbonate, although there are some basaltic and red sandstone (probably from the  
241 underlying Palaeozoic strata) clasts present. Above this basal conglomerate there is a sequence of  
242 coarse-grained purplish-red sandstone. Beds are 0.3-3 m thick with sharp bedding plane contacts.  
243 Grain-size is generally very coarse but also conglomeratic and mudstone horizons are present.  
244 Sandstone beds often exhibit normal grading, contain “floating” rounded pebbles (< 20 mm in  
245 general) and pebble stringers that contain predominately serpentinite clasts (derived from the  
246 underlying ophiolite). In general, serpentinite is the main constituent of the sandstones in the Kıcı  
247 Formation (Table 3). Sedimentary structures are common, such as parallel lamination, planar cross-  
248 bedding (< 0.1 m high foresets) and bioturbation (Fig. 8). It should be noted however, that reliable  
249 palaeocurrent measurements could not be determined due to the poor nature of the exposure.

250 Conglomerate beds are clast-supported, with well-rounded clasts of a generally ophiolitic  
251 composition; rare limestone clasts are also present. The conglomerates are either found at the base  
252 of sandstone beds or form laterally discontinuous lenses. There is also an interval with 1.75 m of  
253 mudstone exposed. The bottom 1 m is composed of thin interbeds of white and pale lilac-coloured  
254 chalk and black mudstone, which is overlain by dark grey mudstone containing roots and plant  
255 material.

256 The Lower Miocene succession is also observed to overlie the Eocene limestones above an  
257 erosional unconformity near Gökdere (Fig. 4d); however, no basal conglomerate is present at this  
258 location, only 1.5 m of mixed breccia and red mudstone (Fig. 9). Above this there is ~5 m of  
259 coarse-grained boundstone, composed mostly of large fragments of algal material (Rhodophyta;

260 *Lithophyllum* sp., *Corallina* sp.: Dasycladaceae; *Halimedia* sp.), other bioclastic (Foraminifera;  
 261 *Textularia* sp., *Spiroloculina* sp., *Globigerina* sp., *Amphistegina* sp., *Quinqueloculina* sp.,  
 262 *Triloculina* sp., *Globorotalia* sp., including *G. menardii*, *Rotalia viennotti* and *Miogypsina* sp) and  
 263 some siliciclastic material. Upwards, the sequence is dominated by coarse litharenite and  
 264 conglomerate. Conglomerates are matrix-supported and composed of rounded clasts of dominantly  
 265 ophiolite material (Table 2). Limestone clasts are also present, which occasionally show evidence of  
 266 boring. Clasts are well-rounded and the size varies between beds. Rounded “floating” pebbles are  
 267 very common within the sandstone beds.

268 Higher in the section, sedimentary structures become more common and parallel lamination,  
 269 trough and planar cross-bedding, pebble imbrication and bioturbation are present. Although, current  
 270 indicators are present most are unsuitable for measurement, three measurements on imbricate  
 271 pebbles were measured (080°, 090°, 120°) suggesting an easterly flow. Additionally, there are  
 272 occasional mudstone beds, generally black in colour with a shaley fabric, with abundant plant  
 273 material and rootlets in some horizons. The top of the sequence is poorly exposed but it appears  
 274 that there is an upward transition to the overlying Kepez Formation. The coarse litharenite is light  
 275 purple to red due to the high content of altered serpentinite. Thin-sections reveal that basaltic clasts  
 276 and polycrystalline quartz are also common.

277 To the southwest, at Kanlidere, the Lower Miocene is markedly different, there ~40 m of  
 278 Lower Miocene sediments outcrop. Fine- to medium-grained, poorly sorted, massive brown  
 279 sandstone is exposed (Fig. 6a), containing unidentified gastropods, fragmented and reworked  
 280 *Corallina* sp and *Lithophyllum* sp., algae, and some foraminifera (*Triloculina* sp., *Neoalveolina* sp.,  
 281 *Spiroloculina* sp., and unidentified Rotaliina). Interbedded with the massive sandstone there are  
 282 three conglomerate horizons (Fig. 6a). These conglomerates are clast-supported, poorly sorted with  
 283 well-rounded to sub-rounded clasts up to 0.4 m in size (Fig. 10a). The matrix is composed of fine-  
 284 grained, brown sandstone, similar to the rest of the exposure and the clasts have a mixed  
 285 composition of limestone and ophiolite (Table 2). Many of the limestone clasts exhibit *Lithophaga-*

286 like borings. The top of the formation is conformable with the overlying limestone (Middle  
287 Miocene Kepez Formation).

288 The Lower Miocene, near Serinyol, is different again. The sediments here are composed of  
289 30 - 40 m of red and brown mottled mudstones with abundant caliche nodules and palaeosol  
290 horizons (Fig. 6b). However, individual beds cannot be distinguished due to the heavily weathered  
291 and diagenetically altered nature of the sediments. No conglomerate was observed in this section.

### 292 3.2.1 *Interpretation*

293 Although there is no dating evidence for this formation, the stratigraphic position below the  
294 Kepez Formation suggests an Early Miocene age and foraminifera identified in the basal bioclastic  
295 facies observed at Gökdere, confirm a Miocene age for the base of the formation. The sedimentary  
296 characteristics of the K1c1 Formation can be broadly differentiated into three facies associations;  
297 alluvial fan, braided stream and shoreline.

298 The presence of both matrix- and clast-supported conglomerates at the base of the type  
299 section, is suggestive of both debris-flow and sheet flood processes. Using standard nomenclature  
300 (Miall, 1978; 1985; 1996) these sediments can be classified as Gmm and Gcm facies, indicating a  
301 SG facies association, interpreted as coarse alluvial fan sediments. The disorganised fabric, large  
302 clast sizes and matrix-supported intervals indicate deposition on a debris flow dominated alluvial  
303 fan (Postma, 1986; Blair and McPherson, 1994). There is no fossil material present, consistent with  
304 a non-marine origin.

305 In contrast, the basal sediments consisting of 1.5 m of breccia and palaeosols at Gökdere,  
306 probably formed through exposure and weathering of the underlying limestone. This is overlain by  
307 microbial boundstone; fossil content indicates a shallow-marine origin for this material with some  
308 reworking and abrasion causing fragmentation of the bioclasts. The encrusting nature of the  
309 Rhodophyta (red algae) caused biological binding of the carbonate and suggests a high-energy  
310 shallow-marine setting (Wright and Burchette, 1996), such as the edge of an algal reef.

311           The upper part of the Lower Miocene is composed of conglomerate and coarse litharenites  
312 with occasional mudstone horizons. However, the type section is a fining-upwards sequence (Fig.  
313 7), whereas a coarsening-up sequence is identified at Gökdere (Fig. 9). Conglomerate horizons  
314 generally occur at the base of sandstone beds or as laterally discontinuous lenses at the type section.  
315 By contrast, there is a higher proportion of conglomerate present at Gökdere. The limestone clasts  
316 locally show evidence of *Lithophaga*-like boring, indicating that some pebbles were reworked in a  
317 shallow marine setting before being incorporated into the these conglomerates, as *Lithophaga* sp.  
318 live in the littoral zone of marine coasts.

319           The cross-bedded sandstones with basal lags of conglomerate seen at the type location are  
320 suggestive of lateral and downstream accretion macroforms and possibly sandy bedforms,  
321 suggesting possible deposition from a braided coarse-grained to sandy bedload river (Miall, 1996).  
322 The fine-grained sediments consisting of soft dark grey to black mudstone indicates high organic  
323 matter content indicative of water-logged conditions. The presence of rootlets and plant material  
324 suggests non-marine conditions and colonisation by plants, indicating deposition on a flood plain,  
325 abandoned channel, or marsh adjacent to the active channel.

326           By contrast, the sandstone exposed at Kanlidere contains bioclastic material including  
327 coralline algae, gastropod and bivalve fragments, and both benthic and planktic foraminifera,  
328 indicating a marine (possibly a shallow-marine peri-reefal) environment. The massive nature of the  
329 sandstone suggests that it has undergone intense bioturbation. Three clast-supported conglomerate  
330 beds are interbedded with the sandstone (Fig. 6a), suggesting a stream-flow or tractional reworking  
331 and winnowing and deposition in a coastal setting. Some of the limestone clasts have borings, also  
332 indicating reworking in a shallow-marine environment prior to deposition. The features described in  
333 these sediments may indicate deposition in the lower shoreface. The mudstones near Serinyol,  
334 interpreted as a palaeosol succession (Fig. 6b), indicate this area was emergent and undergoing soil  
335 formation during the Early Miocene.

336 In addition to the shoreface deposits at Kanlidere, there is evidence of marine influence (i.e.  
337 basal boundstone) at Gökdere, suggesting that this location was proximal to the coast unlike the  
338 type section and represents a regressive sequence. This could imply that these locations represent a  
339 lateral transition of alluvial fan-braided/meandering river-deltaic environments. Therefore, these  
340 facies associations indicate a range of depositional environments along a coarse-grained gravel rich  
341 coast as evidenced by the interaction of marine and alluvial processes. This coarse-grained coast  
342 appears to evolve over time from an alluvial fan delta to a braid delta (Orton, 1988) reflecting the  
343 change in the feeder system from a point sourced alluvial fan to a braided river system (feeder  
344 system types A and B of Postma, 1990). It is not clear whether this fan-delta system is a low  
345 gradient shelf-type, shallow water delta or a slope-type, deep water delta (Postma, 1990) as the pro-  
346 delta sediments have not been identified.

347 The composition of the sandstone of the K1c1 Formation is dominated by serpentine, basalt  
348 and radiolarian chert clasts and there is very little matrix or cement present. This indicates that the  
349 sediment source was probably the underlying ophiolite and related rocks. In contrast, the  
350 conglomerate horizons at Kanlidere were dominantly derived from the sedimentary cover (mainly  
351 limestone and chert). Fine-grained sediments contain abundant quartz and muscovite; these  
352 minerals could be extrabasinal as mica, especially, is uncommon in the local basement rocks.

353

### 354 **3.3 Middle Miocene - Kepez Formation: limestone.**

355 The Kepez Formation is poorly exposed only at a few locations. Near Kepez Hill (adjacent to  
356 Gökdere village), the Middle Miocene is a small exposure of rubblely limestone. This is composed  
357 of shallow-marine debris, such as fragments of oncolite, coral, bivalves, gastropods and echinoids.  
358 Additionally, a large amount of coralline (mainly poritid corals) debris is strewn about the hillside  
359 in this area.

360 Near Kırıkhan, there is a small outcrop of fine-grained crystalline wackestone containing  
361 fragmented coralline algae, foraminifera and echinoids. This bed is variable in thickness (2-3 m)

362 and has an uneven basal surface. This overlies an extremely poorly exposed soft marly limestone.  
363 By contrast, 10-15 m of Middle Miocene limestone is well exposed at Kanlidere (Fig. 6a). The  
364 basal beds are marly wackestone and pass upwards into hard packstone. There is abundant  
365 bioclastic debris, bivalve fragments, bryozoa, echinoids, small gastropods, coral and oncolites.

366 The Middle Miocene exposure near Serinyol is irregular and of a variable thickness (2 to 6  
367 m) composed of recemented rubblely material. Blocks are ~10cm in size, angular and clast-  
368 supported. The limestone is rich in bioclastic material, such as *Pecten*, *Ostrea*, poritid corals and  
369 gastropods (Fig. 10b). Underlying this material there is an irregular basal bed of limestone rich in  
370 fragmented bivalves.

371

### 372 3.3.1 Interpretation

373 These limestones are very poorly exposed and the bioclastic material is fragmented;  
374 therefore, there is little information on which to base an environmental reconstruction. Generally,  
375 the bioclastic packstone indicates formation in shallow-marine conditions, which possibly  
376 accumulated slightly offshore as the fragmentation of the bioclastic material indicates that it was  
377 reworked. Also, the large blocks of limestone seen in the north are characteristic of reef talus.

378 The large coral fragments and the rubblely nature of the limestone, near Serinyol, indicate  
379 that this may also be reef talus, confirming the presence of shallow-marine reefs. As this facies is  
380 observed in a number of different locations (Fig. 3) and as large fringing reefs are uncommon in the  
381 Mediterranean during the Miocene (Franseen et al., 1996), it is most likely that this material was  
382 derived from small patch reefs.

383

## 384 3.4 Upper Miocene mudstone with sandstone interbeds - Gökdere Formation.

385 The type section of the Upper Miocene at Gökdere is composed of fine-grained, grey marl  
386 (Figs. 10c, 12; Table 4). Near the base of the formation are thin (50 mm) interbeds of fine-grained  
387 micaceous litharenite (Table 3). Some of these thin beds exhibit parallel laminations and contain



388 plant fragments, small gastropods and ostracods, but marl sampled for faunal studies were barren.  
389 Upwards the proportion of sand increases; sandstone beds become thicker (< 0.5 m) and more  
390 abundant (Fig. 10d). Sandstone beds are usually found in packets with a significant thickness of  
391 marl between. The sandstone is laterally discontinuous with sharp upper and lower bedding  
392 surfaces. There are an abundance of sedimentary structures present in the sandstones, including  
393 small channel structures, parallel lamination, cross-bedding, ripples, rip-up clasts, load casts, and  
394 current-aligned plant material.

395         The proportion of sand continues to increase upwards until bedding thickness exceeds 1 m;  
396 these beds continue to be interbedded with marl. Near the top of the exposed sequence thin micritic  
397 carbonate horizons are interbedded with the sandstone and marl (Fig. 11). The sandstone weathers  
398 orange and sedimentary structures are uncommon; although mud rip-up clasts and bioturbation were  
399 observed. There are many elongate carbonate-cemented concretions. In thin section these massive  
400 litharenites are composed of a range of lithic fragments (dominantly serpentinite and limestone  
401 clasts), quartz, muscovite, biotite and rare glauconite with some clay matrix and sparry calcite  
402 cement. Additionally, there are fragments of transported algal clasts as well as (transported?)  
403 planktic (*Globigerina* sp., *Globigerinoides* sp.) and benthic foraminifera (*Amphistegina* sp., and  
404 indeterminate Rotaliina). Occasional oyster beds are present, where individual *Ostrea* specimens  
405 can exceed 0.2 m in length. *Turitella* gastropods and plant material are present in adjacent beds.  
406 Thin carbonate beds exhibit parallel lamination and, in thin-section, layers of disarticulated  
407 ostracods valves apparently of only two taxa. The ostracod species are undetermined but *Cyprideis*  
408 *seminulum* (Reuss) and *Cyprideis anatolica* (Bassiovini) have been reported from this formation by  
409 Kop (1996).

410         Around the town of Belen and to the south, the Upper Miocene is well exposed, here  
411 composed of interbedded sandstone and marl/mudstone. The mudstone is very fine-grained,  
412 variable in colour and forms the majority of the succession. The litharenite/calcarenite is fine- to  
413 coarse-grained; beds are normally graded and micaceous. Bed thickness is generally < 0.5 m, but

414 most beds are < 0.1 m thick; laterally, these beds are discontinuous, tending to form discrete packets  
415 within the marl. Sedimentary structures are common; parallel laminations, ripples, cross-  
416 laminations were all observed. Fallen blocks reveal that the bases of the beds have various sole  
417 marks (formed by erosion and bioturbation). Fossils are not generally present but *Ostrea* fragments  
418 were identified and plant material is quite common.

419         The basal Upper Miocene sediments near Serinyol are grey marl, containing small bivalves  
420 (undetermined) and foraminifera (*Globigerinoides trilobus* (Reuss); *Orbulina suturalis*  
421 (Brönniman); *Orbulina bilobata* (d'Orbigny); Boulton et al., 2007) and also fragments of larger  
422 bivalves and polyzoans. Upwards, the colour changes to brownish. There are occasional horizons  
423 with parallel laminations but there are no major lithological variations. The upper part of the  
424 formation, includes packages of sandstone beds, these are 10-20 m thick and formed from thin,  
425 irregular beds of medium-grained calcarenite, separated by a similar thickness of marl. Ripples,  
426 planar cross-lamination, tepee structures and rip-up clasts are present. Some fossil material is  
427 present, mostly as fragmented bivalves.

428         Palaeocurrent measurements from this formation were based generally on ripples, sole  
429 marks and, at the type section, from flow-oriented plant debris. Although there is some spread in  
430 palaeocurrent orientation, in general they indicate a southerly to westerly flow (Fig. 12).

431

#### 432 3.4.1 Interpretation

433         The Upper Miocene forms a coarsening-upward sequence. This sequence is interpreted to  
434 represent a progradational shoreline succession, characterised by a shallowing and coarsening-  
435 upwards sequence from marine offshore muds to silt and sand facies of the shoreface (Reading &  
436 Collinson, 1996). The basal sediments dominated by marl deposition are interpreted as basinal  
437 mudstones.

438         Higher in the succession the proportion of sand increases, probably relating to shallowing  
439 and regression. The laterally discontinuous, generally massive beds with erosional bases are likely

440 to be channel fills. Whereas, the more laterally continuous beds that show a wider range of  
441 sedimentary structures, such as parallel laminations, cross-lamination, ripples and rip-up clasts, are  
442 interpreted as storm generated current deposits due to the similarities to the current-modified  
443 turbidite model of Myrow and Southard (1996).

444 At the type section (Fig. 11), the sequence continues to coarsen upwards and biodiversity is  
445 low in some beds with only one species of *Turitella* and occasional large *Ostrea* present. This low  
446 diversity fossil assemblage could suggest a stressed, possibly brackish water, environment but may  
447 also be the result of the preferential dissolution of aragonite post-deposition. However, the presence  
448 of *Ostracoda* probably *Cyprideis* sp., in thin carbonate horizons is indicative of brackish water,  
449 lagoonal or lacustrine environments of very shallow water, < 10 m in depth (Neale, 1988).  
450 Conversely, a more diverse assemblage, albeit reworked, is found in the massive sandstones  
451 indicating that this material was transported from fully marine conditions. These massive beds  
452 could have been deposited in the lower shoreface where bioturbation may have obliterated  
453 sedimentary structures or again they may be tempestite deposits. Palaeocurrent analysis indicates a  
454 general direction of sediment transport to the west/southwest (Fig. 12), suggesting shore-oblique  
455 currents consistent with storm generated deposition (Myrow and Southard, 1996).

456 At locations other than the type section, these upper coarse sandstones and thin carbonate  
457 horizons are absent. This may be because erosion has removed the upper part of the Miocene in  
458 these other localities or that the shoreline was further into the basin and in the subsurface at the  
459 present time.

460 The marls are composed dominantly of argillaceous lime mud but also contain significant  
461 amounts of quartz (Table 4). Quartz is not expected to be present in high volumes if erosion of the  
462 underlying ophiolite is the main sediment source. This suggests that some detritus was being  
463 sourced from other rocks types, possibly from quartzite exposed in the core of the Amanos  
464 Mountains north of Kırıkhan (e.g., Sadan, Sosink, Seydişehir Formations), or from even more  
465 distant sources, such as the Taurides. Muscovite is present in some samples from the Kıcı and

466 Gökdere Formations and is likely to have an extrabasinal source, possibly from metamorphic rocks,  
467 as micaceous rocks are not common in the immediate area.

## 468 **4 Discussion**

### 469 **4.1 Evolution of the north-western Arabian margin**

470

471 The Hatay (Kızıldağ) and Baer-Bassit Ophiolites were emplaced during the Maastrichtian  
472 (Al-Riyami et al., 2002), southwards onto the Arabian margin. Rising eustatic sea-level (Miller et  
473 al., 2005) possibly combined with isostatic regional subsidence following ophiolite emplacement  
474 resulted in a widespread marine transgression across the Arabian platform throughout Palaeocene  
475 and Early Eocene times. Directly to the south of the study area, in the Nahr El-Kabir region of  
476 Syria, Early – Middle Eocene limestones (Fig. 13) are characteristic of open-shelf conditions with  
477 evidence of westward shallowing during the Middle Miocene (Hardenberg and Robertson, 2007).  
478 Similarly, to the southeast of the study area, in the present Hatay Graben, Lutetian sedimentation  
479 was characterised by a marine transgression from intertidal to shallow open marine conditions  
480 (Boulton and Robertson, 2007). However, in the Belen- Kırıkhan area facies are dominated by  
481 turbidites and northward flowing slumps, indicating a depositional position on the outer ramp or  
482 ramp slope of the Neotethys margin (Fig. 14a). This field evidence is in agreement with current  
483 palaeogeographic models of the region for that time (e.g., Meulenkamp and Sissingh, 2003).

484 Chert is common in these facies and similar facies have been observed in Eocene  
485 carbonates in Hatay, Turkey (Boulton and Robertson, 2007), Syria (Hardenberg and Robertson,  
486 2007), Israel (Rosenfeld and Hirsch, 2005) and onshore and offshore Cyprus (Robertson, 1998).  
487 The presence of diagenetic chert is generally attributed to high diatom and radiolarian productivity  
488 either due to upwelling on the Neotethys margin (Boulton and Robertson, 2007) or due to a marine  
489 connection between the Mediterranean and the Indian Ocean (Hardenberg and Robertson, 2007).

490           Following the deposition of the Eocene carbonates there was a period during which folding  
491 and uplift took place (Boulton and Robertson, 2008). It is likely that this deformation explains the  
492 Oligocene hiatus, which formed during the initial continental collision between Eurasia and Arabia.  
493 Evidence collected here indicates that the collision took place sometime between the Lutetian  
494 (youngest platform carbonates in the area) and the Aquitanian (assumed age of the oldest sediments  
495 above the regional unconformity surface). Such deformation has also been recorded for the Hatay  
496 basin to the southeast (Boulton and Robertson, 2007) and recognised to north on the conjugate  
497 margin seen in the east-central Taurides (Karig and Kozlu, 1990), but was not mentioned by  
498 Hardenberg and Robertson (2007) as having effected coeval strata in northern Syria. Interestingly,  
499 although strata of Oligocene-age are not present in the study area or in the Hatay Graben, strata  
500 from this epoch are present elsewhere to the south, in Syria and Jordan, indicating that the hiatus in  
501 sedimentation during the Oligocene was confined to the northernmost margin of the Arabian plate.  
502 This may indicate that the collisional front was located near to the present-day Bear-Bassit area of  
503 northern Syria. It has also been suggested (Hempton, 1985; Sharland et al., 2004) that non-  
504 deposition in these northern areas of the Arabian plate may have resulted from local uplift during  
505 reactivation of structural lineaments related to the Syrian Arc, but it may also be significant that the  
506 Oligocene was a period of low eustatic sea-level (Miller et al., 2005).

507           During the Early-Middle Miocene conglomerates and sandstones were deposited (Fig. 14b).  
508 Basal sediments were deposited in an alluvial fan setting. Alluvial fans typically form in regions of  
509 active deformation where a hinterland with steep relief is separated from a lower relief basin by a  
510 rapid change in slope gradient (Heward, 1978). This may indicate the presence of an active fault at  
511 this time, but there is no supporting evidence for syn-sedimentary tectonic movement so it is  
512 suggested that the fan formed as a result of erosion of mountains rapidly uplifted by initial  
513 continental collision. Upwards there is a transition to a braid delta system, which prograded east-  
514 south eastwards, into a marine embayment in the Amik Plain area (Fig. 14b). Clast sizes are  
515 significantly smaller higher in the section, this decrease through time could be the result of lowered

516 relief. Palaeosols exposed near Serinyol are interpreted as the lateral, terrestrial equivalent to these  
517 sediments deposited in a floodplain environment.

518         The dominant clast lithology of serpentinite in the K1c1 Formation indicates that the  
519 sediment source was the ophiolite emplaced in the Maastrichtian. However, the presence of  
520 limestone clasts identified as being similar to the Eocene facies, indicates that the young carbonates  
521 had already been uplifted and were being eroded; this probably took place during the Oligocene.  
522 The K1c1 Formation can be correlated with Early Miocene braided-river sediments identified in the  
523 Hatay basin to the southeast (Balyatağı Formation; Boulton and Robertson, 2007) that flowed  
524 northwards from the Baer-Bassit Massif, Syria (Fig. 13). This contrasts with a marine signature for  
525 some parts of the Early Miocene sediments in the Kırıkhan area, although a brief marine incursion  
526 in the Early Miocene has been recorded from the Hatay basin as well (Boulton and Robertson,  
527 2007). This implies that regionally there was a marine incursion in the earliest Miocene with a  
528 regressive trend occurring through the Early and Middle Miocene leading to continental deposition  
529 in the Hatay basin and coastal environments to the north.

530         By contrast, Early Miocene sediments to the north of Kırıkhan, in the suture zone of the  
531 orogeny, are significantly different. These are mainly deep water turbidites that thicken southwards  
532 (Lice Formation: Aktas and Robertson, 1984; Karig and Kozlu, 1990; Robertson et al., 2004; Gül,  
533 2006). Sole marks in those Aquitanian sediments indicate an easterly flow direction along an east-  
534 west orientated basin in the northeast, whereas in the Iskenderun basin the dominant flow direction  
535 was to the southwest (Karig and Kozlu, 1990).

536         To the south at this time the Nahr El-Kabir half graben developed separating the Baer-Bassit  
537 Massif in the northeast from the main Arabian shelf to the south and east (Hardenberg and  
538 Robertson, 2007). Sedimentation during this time was dominated by marine carbonates (Fig. 13).  
539 This indicates that Baer-Bassit, Hatay Basin, Amanos range and parts of the southern Karasu Rift  
540 represented a topographic high during the Early Miocene between the shallow marine carbonate  
541 platform to the south and the foreland (Lice and Iskenderun Basins) to the encroaching collisional

542 front to the north. This is in agreement with Boulton and Robertson (2007) who proposed that the  
543 Early Miocene sediments in the Hatay Basin represented erosion of the flexural forebulge created  
544 by tectonic loading of the subducting slab accentuated by reactivation of basement structures.

545 The Middle Miocene saw the development of localised patch reefs in the study area (Fig.  
546 14c), which pass laterally and vertically up into a coarsening-up sequence of marl to sandstone. The  
547 presence of patch-reefs indicates suitable conditions for coral growth; however, these conditions  
548 were short lived possibly due to the influx of fine-sediment stifling coral growth. The overlying  
549 marl sequence has been dated as Serravallian to Messinian in age (Kozlu, 1982) and the patch reefs  
550 as Langhian–Serravallian (Kozlu, 1982). The marls are marine in the south near Serinyol, however,  
551 the presence of *Ostrea* sp., *Cyprideis* sp., and *Turitella* sp., suggests a restricted marine to brackish  
552 water-environment in the north, at the top of the succession, indicating a shallowing in water depth  
553 to the northeast (Fig. 14d).

554 This sequence shares many similarities to the sediments in the Hatay area, although faulting  
555 related to the formation of the Hatay Graben appears to have initiated during the Middle Miocene  
556 (Boulton et al., 2006) the area was still part of the wider foreland basin to the thrust front (Boulton  
557 and Robertson, 2007). Sedimentation during the Langhian and Serravallian was dominated by  
558 shallow-marine peritidal carbonate deepening up into outer ramp carbonates and then marls over  
559 time possibly due to flexural subsidence relating to foreland loading (Boulton and Robertson,  
560 2007). Patch reefs were identified in the northwest of that area (near Kesecik, Boulton and  
561 Robertson, 2007; their figure 1), close to the area discussed in this paper indicating that the study  
562 area was also part of the shallow underfilled foreland basin of the collisional zone. It is possible that  
563 subsidence was greater in the southeast due to the effect of local normal faulting superimposed on  
564 regional subsidence; whereas the absence of normal faulting in areas to the north reduced overall  
565 subsidence rates and the resulting accommodation space.

566 However, the marls of the Hatay and Karasu sequences differ in composition with higher  
567 concentration of quartz and mica present in the sediments around Kırıkhan, whereas mica is

568 uncommon in the Hatay Graben and quartz concentrations are much lower (Boulton, 2006). This  
569 implies that the Hatay Graben was more distal from these detrital sediment sources than the  
570 Kırıkhan area. The quartz could have been eroded locally but there are no micaceous basement  
571 rocks in the vicinity suggesting that this material was transported from a greater distance. The  
572 nearest outcropping micaceous rocks are to the north of the suture zone, in the Berit region  
573 (described in detail by Robertson et al., 2006) some 150 km from the study area, there mica schists  
574 and granites outcrop. This suggests that by the Late Miocene, sediment eroded from north of the  
575 suture was being transported across the suture zone into the foreland basin that developed in front of  
576 the leading edge of the collision.

577 By contrast, to the south, in present day Syria, the main development of the Nahr El-Kabir  
578 half-graben took place in the Middle Miocene (Hardenberg and Robertson, 2007). There is a Late  
579 Serravallian thin chalk horizon present, but there are no sediments of Tortonian age present (Fig.  
580 13). Hardenberg and Robertson (2007) explain this as due to local tectonics influencing  
581 sedimentation. Unlike the Hatay and Nahr El-Kabir areas, evidence for syn-sedimentary faulting  
582 has not been observed in Middle-Late Miocene sediments around Kırıkhan, Belen or Serinyol.

583 Messinian evaporites are not present in this area, although they have been identified to the  
584 north in the Iskenderun Bay (Boulton, 2006), in the Hatay Graben (Boulton et al., 2006; Boulton  
585 and Robertson 2007) and to the south in Syria (Hardenberg and Robertson, 2007). It is not clear  
586 whether evaporites were either not deposited in the area, were deposited and subsequently eroded,  
587 or are buried in the subsurface.

588 Pliocene sediments have not been identified around Kırıkhan, Belen or Serinyol, existing  
589 micropalaeontological dating indicates the youngest sediments near Serinyol are of Late Miocene  
590 age (Boulton et al., 2007). Pliocene sediments are present to the southeast in the Hatay Graben  
591 (Boulton et al., 2006) and to the south in the Nahr El-Kabir Graben (Hardenberg and Robertson,  
592 2007) but both of these were tectonically active basins during the Neogene, whereas the Kırıkhan  
593 area was not. It is likely that regional Pliocene-Recent uplift, related to continued convergence



594 between Arabia and Anatolia, induced terrestrial deposition earlier in the Kırıkhan-Karasu region,  
595 compared to areas to the south and west (Fig. 14e).

596 In addition to regional uplift, the DSFZ propagated northwards during the Pliocene.  
597 Transtension resulted in strike-slip and extensional components of deformation (Boulton, in  
598 review), the extensional component of deformation caused flank uplift and basin floor subsidence  
599 leading to the formation of the present topographic graben. The lack of dated Pliocene sediments  
600 and a Quaternary age for the rift fill suggests that significant topography did not develop until the  
601 Late Pliocene. Subsequently, up to ~350 m of Pleistocene river gravel (mostly unexposed) have  
602 accumulated within the Karasu Rift (Rojay et al., 2001). Moreover, some 11 inactive alluvial fans  
603 are interbedded with basalts that have yielded dates ranging from 1.57 – 0.05 Ma (Rojay et al.,  
604 2001; Yurtmen et al., 2002; Tatar et al., 2004). These basalts are associated with volcanic necks and  
605 have been attributed to block rotations and extension of the Karasu Rift (Tatar et al., 2004).

606

#### 607 **4.2 Timing of continental collision and implications**

608 The Amanos Mountains are located at the westernmost interface between an extensive mobile  
609 belt to the east that has been deformed and uplifted following the closure of the southern Neotethys  
610 Ocean and consequent Arabia-Eurasia collision, and an extensive area to the west that has yet to  
611 undergo full continental collision (Mediterranean Basin). The study area is also located to the south  
612 of the Bitlis suture zone (Fig. 1). Constraining the timing of deformation, initial uplift and  
613 subsequent evolution of the southern Karasu Rift allows this area to be integrated into the broader  
614 geotectonic framework and enhances our understanding of the orogenic evolution in this sector of  
615 the Alpine-Himalayan chain.

616 In the East, south of the Zagros suture zone, collision has been shown to have commenced in  
617 the Late Eocene to Oligocene. Agard et al., (2005) constrained the timing of collision to between  
618 35 and 25-23 Ma; after the last intrusion of mafic igneous material related to arc volcanism and  
619 prior to the onset of Late Oligocene/Early Miocene sedimentation. This is corroborated by the work

620 of Hassami et al., (2001) on progressive unconformities in the Zagros that indicate deformation  
621 began in the Late Eocene. Further to the west in northern Iraq, terrestrial clastics dated to the Late  
622 Eocene have been inferred to represent sub-aerial uplift and erosion of the northeastern edge of the  
623 Arabian plate by this time (Dhannoun et al., 1988). Collectively, these data corroborate the  
624 findings from the Karasu Rift and Hatay Graben, where folded Eocene and older strata underlie an  
625 extensive hiatus of Oligocene indicating that compressional deformation along the north Arabian  
626 margin was taking place from the Late Eocene onwards.

627 Similarly, evidence from the north of the suture zone in the Caucasus and Caspian Basin  
628 indicates that the onset of collision also took place during the Late Eocene – Oligocene (Patton,  
629 1993; Vincent et al., 2005; 2007) due to the presence of deformed and eroded Eocene strata  
630 unconformably overlain by clastics of presumed Oligocene age, olistostromes and compressional  
631 deformation observed in the subsurface. Late Eocene uplift has also been recorded in northern Iran  
632 (Alborz), where a Middle Eocene basin was inverted by the Early Oligocene (Alvavi, 1996; Guest  
633 et al., 2006).

634 In southern Turkey, north of the Bitlis suture zone, structural, sedimentological and  
635 stratigraphical studies have determined that the initial collision took place between the Late Eocene  
636 (Yilmaz, 1993) and Early Miocene time. Robertson et al., (2004; 2006) proposed that diachronous  
637 oblique subduction continued throughout the Eocene and that olistostromes indicate that the latest  
638 stages of subduction and initial collision took place in the Oligocene to Early Miocene. In many  
639 central Anatolian basins, sedimentation continued through the Late Eocene but was terminated by a  
640 basal Oligocene unconformity that is present in nearly all basins (e.g., Şarkışla basin, Gökten, 1986;  
641 Sivas basin, Dilek et al., 1999; Ulukisla basin, Clark and Robertson, 2005; Tuzgölü basin, Görür et  
642 al., 1989). In addition, latest Eocene folding is also reported for these same areas indicating that  
643 deformation propagated rapidly northwards into the interior of the Anatolian plate, as well as  
644 propagating rapidly northwards into the interior of the Eurasian Plate (Vincent et al., 2005; 2007).  
645 Alternatively, deformation initiation took place over a wide area.

646 The evidence present here, supports that from the region and shows that widespread  
647 deformation took place during the Late Eocene to Oligocene from Iran to western Anatolia. This  
648 indicates that the closure of the southern Neotethys and initial continental collision took place  
649 almost simultaneously along the entire frontal sector of the Arabian Plate with associated  
650 deformation propagating rapidly into the hinterland. This suggests that rather than the collision  
651 being diachronous in nature, it was broadly synchronous along the leading edge of the Arabian  
652 Plate.

653 Interestingly, the Eocene to earliest Oligocene was also a period of rapid expansion of the  
654 Antarctic continental ice sheet (Zachos et al., 2001); the closure of the Tethys Ocean in conjunction  
655 with other oceanographic changes, such as the widening of the North Atlantic Ocean (Zachos et al.,  
656 2001), would seem to be a significant factor in the climatic changes that occurred at the Eocene-  
657 Oligocene boundary.

## 658 **5 Summary and Conclusions**

659 Deposition of the Cenozoic sediments exposed in the Amanos Mountains, was dominantly  
660 controlled by subsidence related to continental collision taking place to the north and concomitant  
661 foreland basin formation south of the suture zone. The study area represents a Late Cretaceous to  
662 Eocene north-facing continental shelf at the southern Neotethys passive continental margin.. The  
663 Late Eocene to Oligocene is absent in the area due to erosion or non-deposition of sediments  
664 indicating that during some, if not all, of this period the area was uplifted and eroded. This uplift is  
665 attributed to the flexure of the crust and southward migration of the flexural bulge resulting from  
666 loading of the Arabian lithosphere due to continental closure of the Neotethys to the north. Recent  
667 research (e.g., Patton, 1993 Vincent et al., 2005; 2007; Allen and Armstrong, 2008) indicates that  
668 initial continental collision appears to have taken place nearly simultaneously along the leading  
669 edge of Arabia. Although, high resolution studies need to be undertaken to confirm this as the Late

670 Eocene to end Oligocene is a period of some 20 Ma and diachronism of the continental collision  
671 cannot be excluded completely.

672 Continental sedimentation during the Early Miocene reflects erosion of uplifted areas due to  
673 regional deformation resulting from the final closure of the Neotethys and suture tightening along  
674 the Misis-Andırın lineament. The flexural bulge passed to the south of the area and was shedding  
675 material northwards into the foreland basin; however, the proto-Amanos Mountains appear to  
676 already have developed into a topographic high and were additionally shedding sediment  
677 southwards. Marine transgression during the Middle to Late Miocene resulted in the deposition of  
678 localised patch reefs and clastic sediments were deposited into local depocentres (i.e., Hatay basin,  
679 Amik basin) with palaeocurrents directed to the south and west, indicating that the palaeoslope was  
680 orientated towards the developing Hatay Graben and not northwards towards the thrust front.

681 Regional uplift combined with a general regressive trend resulted in continental conditions by  
682 the latest Miocene/Pliocene that continue to the present day. Transtension, related to the  
683 northwards propagation of the DSFZ, resulted in the formation of the Karasu Rift during the  
684 Pliocene. The extensional component of deformation created accommodation space and fluvial  
685 conglomerates accumulated within the axial zone of the rift. These sediments are interbedded with  
686 lavas that resulted from localised extension and block rotations in the rift floor.

687

## 688 **Acknowledgements**

689 My thanks go to Malcolm Hart for foraminiferal identifications and to Alastair Robertson and  
690 Matthew Watkinson who commented on earlier versions of this manuscript. Additionally, the  
691 suggestions of the editor Gert Jan Weltje, Johan ten Veen and an anonymous reviewer greatly  
692 improved this manuscript. This work was initiated during a NERC PhD studentship at the  
693 University of Edinburgh and completed at the University of Plymouth with funding from the Royal  
694 Society.

695

696 **References**

697 Adiyaman, O., Chorowicz, J., 2002. Late Cenozoic tectonics and volcanism in the north western  
698 corner of the Arabian Plate: a consequence of the strike-slip Dead Sea Fault zone and the lateral  
699 escape of Anatolia. *Journal of Volcanology and Geothermal Research*, 117, 327-345.

700

701 Agard, P., Omrani, J., Jolivet, L., Mouthereau, F., 2005. Convergence history across Zagros (Iran):  
702 constraints from collisional and earlier deformation. *International Journal of Earth Sciences*, 94,  
703 401-419.

704

705 Aktas, G., Robertson, A.H.F., 1984. The Maden Complex, S E Turkey: evolution of a Neotethyan  
706 continental margin. In: Dixon, J.E., Robertson, A.H.F. (Eds.). *The Geological Evolution of the*  
707 *Eastern Mediterranean*. Geological Society, London, Special Publications, 17, 375-402.

708

709 Akyuz, H. S., Altunel, E., Karabacak, V., Yalciner C. C., 2006. Historical earthquake activity of  
710 the northern part of the Dead Sea Fault Zone, southern Turkey. *Tectonophysics*, 426 (3-4), 281-  
711 293.

712

713 Allen, M. B., Armstrong, H. A., 2008. Arabia-Eurasian collision and the forcing of mid Cenozoic  
714 global cooling. *Palaeogeography, Palaeoclimatology Palaeoecology*, doi:  
715 10.1016/j.palaeo.2008.04.021

716

717 Alavai, M., 1996. Tectonostratigraphic synthesis and structural style of the Alborz mountain  
718 system in northern Iran. *Journal of Geodynamics*, 21, 1-33.

719

720 Al-Riyami, K., Robertson, A.H.F., Dixon, J.E, Xenophontos, C., 2002. Origin and emplacement of  
721 the Late Cretaceous Baer-Bassit ophiolite and its metamorphic sole in NW Syria, *Lithos*, 65, 225-  
722 260.

723

724 Arger, J., Mitchell, J., Westaway, R., 2000. Neogene and Quaternary volcanism of south-eastern  
725 Turkey. In: Bozkurt, E., Winchester, J. A., Piper, J. D. A. (eds). *Tectonics and Magmatism of*  
726 *Turkey and the Surrounding Area*. Geological Society, London, Special Publications, 173, 459-487.

727

728 Atan, O. R. 1969. Egribucak Kirikhan bölgesindeki ofiyolilerin jeolojisi ve petrografisi [Geology  
729 and Petrography of the Kirikhan District Ophiolite]. M.T.A yayini no 150, pp71, Ankara.

730

731 Beyarslan, M., Bingöl, A. F., 2000. Petrology of a super-subduction zone ophiolite (Elazığ  
732 Turkey). *Canadian Journal of Earth Sciences*, 37, 1411-1424.

733

734 Blair, T.C., McPherson, J.G., 1994. Alluvial fans and their natural distinction from rivers based on  
735 morphology, hydraulic processes, sedimentary processes, and facies assemblages. *Journal of*  
736 *Sedimentary Research*, A64, 450-489.

737

738 Boulton, S. J., Transpression or transtension? Structure of the northern Dead Sea Fault Zone. In  
739 review for *Journal of Structural Geology*.

740

741 Boulton, S. J., 2006. Tectonic-sedimentary evolution of the Cenozoic Hatay Graben, South Central  
742 Turkey. University of Edinburgh, unpublished PhD thesis, 414pp.

743

- 744 Boulton, S. J., Robertson, A. H. F., 2007. The Miocene of the Hatay area, S Turkey: Transition  
745 from the Arabian passive margin to an underfilled foreland basin related to closure of the Southern  
746 Neotethys Ocean. *Sedimentary Geology*, 198, 93-124.
- 747
- 748 Boulton, S. J., Robertson, A. H. F., Unlügenç, Ü. C., 2006. Tectonic and sedimentary evolution of  
749 the Cenozoic Hatay Graben, Southern Turkey: A two-phase, foreland basin then transtensional  
750 basin model. In: Robertson, A.H.F., Mountrakis, D. (eds.), *Tectonic Evolution of the Eastern  
751 Mediterranean*. Geological Society, London, Special Publications, 260, 613-634.
- 752
- 753 Boulton, S. J., Robertson, A. H. F., Ellam, R. M., Safak, Ü., Ünlügenç., U. C., 2007 Strontium  
754 isotopic and micropalaeontological dating used to redefine the stratigraphy of the Neotectonic  
755 Hatay Graben, southern Turkey. *Turkish Journal of Earth Sciences*, 16, 141-179.
- 756
- 757 Bouma, A. H., 1962. *Sedimentology of some Flysch deposits: A graphic approach to facies  
758 interpretation*, 168p, Elsevier, Amsterdam.
- 759
- 760 Bull, W. B., 1972. Recognition of alluvial fan deposits in the stratigraphic record. In: Rigby, J.K. &  
761 Hamblin, W. K. (eds) *Recognition of ancient sedimentary environments*. Society of Economic  
762 Palaeontology and Mineralogy Special Publication, 16, 63-83.
- 763
- 764 Çapan, U. Z., Vidal, P., Cantagrel, J. M., 1987. K –Ar, Sr and Pb isotopic study of Quaternary  
765 volcanism in the Karasu valley (Hatay), N-end of the Dead-Sea rift zone in SE-Turkey. *Hacettepe  
766 University Earth Sciences*, 14, 165-178.
- 767

- 768 Clark, M., Robertson, A., 2005. Uppermost Cretaceous – Lower Tertiary Ulukisla Basin, south  
769 central Turkey: sedimentary evolution of part of a unified basin complex within an evolving  
770 Neotethyan suture zone. *Sedimentary Geology*, 173, 15 -51.  
771
- 772 Çogulu, E., 1974. Ultrabasic tectonites and layered peridotites of the Hatay area (Turkey). *Bulletin*  
773 *of the Maden Tektik Arama*, 83, 139-147.  
774
- 775 Dean, W. T., Krummenacher, R., 1961. Cambrian trilobites from the Amanos Mountains, Turkey.  
776 *Palaeontology*, 4, 71-81.  
777
- 778 Dean, W. T., Monod, O., Günay, Y., 1986. Lower Palaeozoic stratigraphy in the southern and  
779 central Amanos Mountains, south central Turkey. *Geological Magazine*, 123 (3), 215-226.  
780
- 781 Delaloye, M., Piskin, Ö., Selçuk, H., Vuagnat, M. & Wagner, J-J. 1980. Geological section through  
782 the Hatay ophiolite along the Mediterranean coast, southern Turkey. *Ofiliti*, 52 (3), 205-216.  
783
- 784 Dhannoun, H. Y., Aldabbagh, S. M. A., Hasso, A. A., 1988. The geochemistry of the Gercus Red-  
785 bed formation of Northeast Iraq. *Chemical Geology*, 69, 87-93.  
786
- 787 Dilek, Y., Thy, P., Hacker, B., Grundvig, S., 1999. Structure and petrology of Tauride ophiolites  
788 and mafic dike intrusions (Turkey): implications for the Neotethyan ocean. *Geological Society of*  
789 *America Bulletin*, 111, 1192– 1216.  
790
- 791 Dokumaci, Y., 1997. Belen tektono-stratigrafik incelemesi (Tectono-stratigraphic investigations of  
792 the Belen area). MSc. Thesis, University of Çukurova.  
793



- 794 Dubertret, L. 1939. Sur la genèse et l'âge des roches vertes syriennes. Comptes Rendus de  
795 l'Académie des Sciences, Paris, 209 P763.  
796
- 797 Dubertret, L. 1953. Géologie des roches vertes du nord-ouest de la Syrie et du Hatay (Turquie).  
798 Notes et Mémoires sur le Moyen-Orient, Museum Nationale et histoire naturelle, 5, 5-179, Paris.  
799
- 800 Franseen, E. K., Esteban, M., Ward, W. C., Rouchy, J-M., 1996. Models for carbonate stratigraphy  
801 from Miocene reef complexes of Mediterranean regions. Society for Sedimentary Geology –  
802 Concepts in Sedimentology and Paleontology Volume 5, 391pp  
803
- 804 Garfunkel, Z., Ben-Avraham, Z., 1996. The structure of the Dead Sea Basin. Tectonophysics, 255,  
805 155-176.  
806
- 807 Garfunkel, Z., Zak, I., Freund, R., 1981. Active Faulting in the Dead Sea Rift. Tectonophysics, 80,  
808 1-26.  
809
- 810 Gökten, E., 1986. Palaeocene carbonate turbidites of the Şarkışla region, Turkey—their significance  
811 in an orogenic basin. Sedimentary Geology 49, 143– 165.  
812
- 813 Görür, N., Tüysüz, O., Şengör, A.M.C., 1998. Tectonic evolution of the Central Anatolian Basins.  
814 International Geological Review, 40, 831–850.  
815
- 816 Guest, B., Stockli, D. F., Grove, M., Axen, G. J., Lam, P. S., Hassanzadeh, J., 2006. Thermal  
817 histories from the central Alborz Mountains, northern Iran: Implications for the spatial and temporal  
818 distribution of deformation in northern Iran. Geological Society of America Bulletin, 118, 1507 –  
819 1521.

820

821 Gül, M., 2006. Evolution of the turbidite system in the Kahramanmaraş Basin. Cükürova

822 University, Unpublished PhD thesis.

823

824 Günay, Y. 1984. Amanos daglarının jeolojisi ve Karasu-Hatay grabeninin petrol olanakları. TPAS

825 Hakkari-Saryaj Projesi, TPAO-1984, Ankara.

826

827 Hall, R., 1976. Ophiolite emplacement and evolution of the Taurus suture zone. South-east

828 Turkey. Geological Society of America, Bulletin, 87, 1078-1088.

829

830 Hardenberg, M., Robertson, A.H.F., 2007. Sedimentology of the NW margin of the Arabian plate

831 and the SW-NE-trending Nahr El-Kabir half-graben in northern Syria during latest Cretaceous-

832 Cenozoic. Sedimentary Geology. Doi: 10.1016/j.sedgeo.2007.02.009

833

834 Hempton, M. R., 1987. Constraints on Arabian Plate motion and extensional history of the Red Sea.

835 Tectonics 6, 687-705.

836

837 Hessami, K., Koyi, H. A., Talbot, C. J., Tabasi, H., Shabanian, E., 2001. Progressive

838 unconformities within an evolving foreland fold-thrust belt, Zagros Mountains. Journal of the

839 Geological Society, London, 158, 969 – 981.

840

841 Heward, A.P., 1978. Alluvial fan sequence and mega sequence models: with examples from

842 Westphalian D-Stephanian B coalfields, northern Spain. In: Maill, A.D. (ed) Fluvial

843 Sedimentology. Canadian Society of Petroleum Geologists, Memoirs, 5, 669-702.

844

845 Holmes, A. 1965. Principles of Physical Geology, 2nd Edition. Nelson, London. Pp 1288.

846

847 Ishmawi, R., 1972. Geologie des nordlichen Mittelteils des Amanos-Gebirges zwischen Islahiye  
848 und Bahçe (S. Türkei). Geotektonischen Forschungen, 42, 34-63.

849

850 Janetzko, P., 1972. Geologische Untersuchungen an der Ostflanke des sudlichen Amanos-Gebirges  
851 zwischen Islahiye und Hassa (Sudtürkei). Geotektonischen Forschungen, 42, 3-33.

852

853 Karig, D. E., Kozlu, H., 1990. Late Palaeogene – Neogene evolution of the triple junction region  
854 near Maraş, south central Turkey. Journal of the Geological Society, London, 147, 1023-1034.

855

856 Kelling, G., Gökçen, S. L., Floyd, P. A., Gökçen, N., 1987. Neogene tectonics and plate  
857 convergence in the eastern Mediterranean: New data from southern Turkey. Geology, 15, 425-429.

858

859 Kop, A., 1996. Kirikhan ve Kuzeyinin tektono-stratigrafik incelemesi (Tectono-stratigraphic  
860 investigations of Kirikhan and its northern area). MSc Thesis, University of Çukurova, Turkey.

861

862 Kozlu, H. 1982. İskenderun Baseni Anadolu nun Kambrien teşekkülleri ve bunların Doğu İran  
863 Kambrieni ile mukayesesi. MTA periodical no 66, Ankara.

864

865 Kozlu, H., 1997. Tectono-stratigraphic units of the Neogene basins (Iskenderun, Misis-Andirin) and  
866 their tectonic evolution in the eastern Mediterranean region. [PhD Thesis] Natural Science Institute,  
867 Cukurova University, Turkey.

868

869 Lahner, L., 1972. Geologische Untersuchungen an der Ostflanke des des mittleren Amanos (SE  
870 Türkei). Geotektonischen Forschungen, 42, 64-96.

871

872 Lyberis, N., 1988. Tectonic evolution of the Gulf of Suez and the Gulf of Aqaba. *Tectonophysics*,  
873 153 (1-4), 209-220.

874

875 Miall, A. D., 1978. *Fluvial Sedimentology*. Canadian Society of Petroleum Geologists Memoir, 5,  
876 859pp.

877

878 Miall, A. D., 1985. Architectural element analysis: a new method of facies analysis applied to  
879 fluvial deposits. *Earth-Science Reviews*, 22, 261-308.

880

881 Miall, A. D., 1996. *The Geology of Fluvial Deposits: Sedimentary facies, basin analysis and*  
882 *petroleum geology*. Springer-Verlag, Berlin, 582 pp.

883

884 Miller, K. G., Kominz, M. A., Browning, J. V., Wright, J. D., Mountain, G. S., Katz, M. E.,  
885 Sugarman, P. J., Cramer, B. S., Christie-Blick, N., Pekar, S. F., 2005. The Phanerozoic record of  
886 global sea-level change. *Science*, 310 (5752), 1293-1298.

887 Meulenkamp, J. E., Sissingh, W., 2003. Tertiary palaeogeography and tectonostratigraphic  
888 evolution of the Northern and Southern Peri-Tethys platforms and the intermediate domains of the  
889 African-Eurasian convergent plate boundary zone. *Palaeogeography, Palaeoclimatology,*  
890 *Palaeoecology*, 196, 209-228.

891

892 Myrow, P.M., Southard, J.B., 1996. Tempestite deposition. *Journal of Sedimentary Research*, 66  
893 (5), 875-887.

894

895 Neale, J.W., 1988. Ostracods and palaeosalinity reconstruction. In: De Deckker, P. Colin, J.-P.,  
896 Peypouquet, J.P., (Eds), *Ostracoda in the Earth Science*, Elsevier, Amsterdam, pp. 125–155.

897

- 898 Nilsen, T. H., 1982. Fluvial Models. In: Sandstone Depositional Environments, Ed. P.A. Scholl &  
899 D. Spearing. pp115-137. AAPG Memoir 31.  
900
- 901 Orton, G.J., 1988. A spectrum of Middle Ordovician fan deltas and braidplain deltas, North Wales:  
902 a consequence of varying fluvial clastic input. In: Nemeč, W., Steel, R.J. (Eds) Fan Deltas:  
903 Sedimentology and Tectonic Settings. Blackie, London, 23-49.  
904
- 905 Över, S., Ünlügenç, U. C., Bellier, O., 2002. Quaternary stress regime change in the Hatay region,  
906 SE Turkey. *Geophysics Journal International*, 148, 649-662.  
907
- 908 Parlak, O., Kop, A., Ünlügenç, U. C., Demirkol, C., 1998. Geochronology and geochemistry of  
909 basaltic rocks in the Karasu graben around Kirikhan Hatay, S. Turkey. *Turkish Journal of Earth  
910 Sciences*, 7, 53-61.  
911
- 912 Patton, D.K., 1993. Samgori field, Republic of Georgia: critical review of island-arc oil and gas.  
913 *Journal of Petroleum Geology*, 16, 153-167.  
914
- 915 Piskin, O., Delaloye, M., Selçuk, H., Wagner, J., 1986. Guide to Hatay Geology SE Turkey.  
916 *Oflioliti*, 11, 87-104.  
917
- 918 Postma, G., 1986. Classification for sediment gravity-flow deposits based on flow conditions during  
919 sedimentation. *Geology*, 14, 291-294.  
920
- 921 Postma, G., 1990. Depositional architecture and facies of rivers and fan deltas: a synthesis. In:  
922 Collela, A., Prior, D.B., (Eds) Coarse-grained deltas. Special Publication of the International  
923 Association of Sedimentologists, 10, 13-27.

924

925 Reading, H. G. & Collinson, J. D. 1996. Clastic coasts. In: *Sedimentary Environments: Processes,*  
926 *Facies and Stratigraphy*, 3rd edition Ed: H.G. Reading. Blackwell Science. 154-231.

927

928 Robertson, A. H. F., 1998. Mesozoic-Tertiary Tectonic evolution of the easternmost Mediterranean  
929 area: integration of marine and land evidence. In: Robertson, A. H. F., Emeis, K.-C., Richter, C.,  
930 Camerlenghi, A. (eds.), *Proceedings of the Ocean Drilling Program, Scientific Results*, 160, 723-  
931 782.

932

933 Robertson, A.H.F., 2000. Mesozoic-Tertiary tectonic-sedimentary evolution of a south Tethyan  
934 oceanic basin and its margins in southern Turkey. In: Bozkurt, E., Winchester, J.A, Piper., J.D.  
935 (eds.), *Tectonics and Magmatism in Turkey and the Surrounding Area.*. Geological Society,  
936 London, Special Publications, 173, 43-82.

937

938 Robertson, A.H.F., 2002. Overview of the genesis and emplacement of Mesozoic ophiolites in the  
939 Eastern Mediterranean Tethyan region, *Lithos*, 65, 1-67.

940

941 Robertson, A. H. F, Dixon, J. E., 1984. Introduction: aspects of the geological evolution of the  
942 Eastern Mediterranean. In: Dixon, J.E., Robertson, A. H. F (eds). *The Geological evolution of the*  
943 *Eastern Mediterranean.* Geological Society , London, Special Publications, 17, 1-74.

944

945 Robertson, A. H. F., Ünlügenç, U. C., Inan, N., Tasli, K. 2004. The Misis-Andirin Complex: a  
946 Mid-Tertiary melange related to late-stage subduction of the Southern Neotethys in S Turkey.  
947 *Journal of Asian Earth Sciences*, 22, 413-453.

948

- 949 Robertson, A. H. F., Ustaömer, T., Parlak, O., Ünlügenç, U. C., Taşlı, K., İnan, N., 2006. The Berit  
950 transect of the Tauride thrust belt, S Turkey: Late Cretaceous – Early Cenozoic  
951 accretionary/collisional processes related to closure of the Southern Neotethys. *Journal of Asian*  
952 *Earth Sciences*, 27, 108-145.
- 953
- 954 Rojay, B., Heimann, A., Toprak, V., 2001. Neotectonic and volcanic characteristics of the Karasu  
955 fault zone Anatolia, Turkey: The transition zone between the Dead Sea transform and the East  
956 Anatolian fault zone. *Geodynamica Acta*, 14, 197-212.
- 957
- 958 Rosenfeld, A., Hirsch, F., 2005. The Paleocene – Eocene of Israel. In: Hall, J. K., Krasheninnikov,  
959 V. A., Hirsch, F., Benjamini, C., Flexer, A. (eds). *Geological Framework of the Levant, Volume II:*  
960 *The Levantine Basin and Israel. Historical Productions – Hall, Jerusalem.* 437-459.
- 961
- 962 Saller, A., Armin, R., Ichram, L.O., Sullivan, C., 1993. Sequence stratigraphy of aggrading and  
963 backstepping carbonate shelves, Oligocene, Central Kalmantan, Indonesia. In: Loucks, R. G., Sarg,  
964 J. F. (eds), *Carbonate Sequence Stratigraphy: Recent developments and Applications.* American  
965 *Association of Petroleum Geologists Memoir*, 57, 267-290.
- 966
- 967 Şaroğlu, F., Emre Ö., & Kuşçu, İ. 1992. The East Anatolian fault zone of Turkey. *Annales*  
968 *Tectonicae*, 6, 99-125.
- 969
- 970 Şengör, A.M.C., Yılmaz, Y., 1981. Tethyan evolution of Turkey: a plate tectonic approach.  
971 *Tectonophysics*, 75, 81-241.
- 972
- 973 Schwan, W., 1971. Geology and tectonics of the central Amanos Mountains. In: Cambell, A.S (ed)  
974 *Geology and History of Turkey. Tripoli: The petroleum Exploration Society of Libya*, 283-303.

975

976 Sharland, P.R., Casey, D.M., Davies, R.B., Simmons, M.D., Sutcliffe, O.E., 2004. Arabian Plate  
977 stratigraphy-revisions to SP2. *GeoArabia*, 9, 199-214.

978

979 Tatar, O., Piper, J. D. A., Gürsoy, H., Heimann, A., Koçbulut, F., 2004. Neotectonic deformation in  
980 the transition zone between the Dead Sea Transform and the East Anatolian Fault Zone, Southern  
981 Turkey: a palaeomagnetic study of the Karasu Rift volcanism. *Tectonophysics*, 385, 17-43.

982

983 Vincent, S. J., Allen, M. B., Ismail-Zadeh, A. D., Flecker, R., Foland, K. A., Simmons, M. D.,  
984 2005. Insights from the Talysh of Azerbaijan into the Paleogene evolution of the South Caspian  
985 region. *Geological Society of America Bulletin*, 11, 1513 – 1533.

986

987 Vincent, S. J., Morton, A. C., Carter, A., Gibbs, S., Barabadze, T. G., 2007. Oligocene uplift of the  
988 Western Greater Caucasus: an effect of initial Arabia-Eurasia collision. *Terra Nova*, 19, 160-166.

989

990 Westaway, R., 2003. Kinematics of the Middle East and Eastern Mediterranean updated. *Turkish  
991 Journal of Earth Sciences*, 12, 5-46.

992

993 Westaway, R., Arger, J., 2001. Kinematics of the Malatya-Ovacik fault zone. *Geodynamica Acta*,  
994 14, 103-131.

995

996 Wright V. P & Burchette, T. P. 1996. Shallow water carbonate environments. In: *Sedimentary  
997 Environments: Processes, Facies and Stratigraphy*, 3rd edition Ed: H.G. Reading. Pp. 325-394.  
998 Blackwell Science.

999



- 1000 Yılmaz, Y., Yiğitbaş, E., Genç, S. C., 1993. Ophiolitic and metamorphic assemblages of southeast  
1001 Anatolia and the significance in the geological evolution of the orogenic belt. *Tectonics*, 12, 1280-  
1002 1297.
- 1003
- 1004 Yurtmen, S., Guillou, H., Westaway, R., Rowbotham, G., Tatar, O., 2002. Rate of strike-slip  
1005 motion on the Amanos Fault (Karasu Valley, southern Turkey) constrained by K-Ar dating and  
1006 geochemical analysis of Quaternary basalts. *Tectonophysics*, 344, 207-246.
- 1007
- 1008 Zachos, J. C., Pagani, M., Sloan, E. T., Billups, K., 2001. Trends, rhythms, and aberrations in global  
1009 climate 65 Ma to present. *Science*, 292, 686-694.
- 1010

1011

1012 **Tables**

Name	Age	Lithology	Boundaries	Thickness
Gökdere Fm	Tortonian - Messinian	Marl and litharenite	Conformable with Kepez Fm or unconformable on or faulted against older units. Upper boundary to younger sediments not exposed.	400 – 700m
Kepez Fm	Langhian	Wackestone and packstone	Lower boundary unconformable on K1c1 or conformable with Gökdere, upper transitional to Gökdere Fm.	15m
K1c1 Fm	Aquitanian – Burdigalian	Conglomerates, litharenites and mudstones	Unconformable with units above and below. Also fault contacts with Gökdere Fm	100 - 150m
Hacıdağ Fm	Palaeocene - Eocene	Calcarenite, wackestone, packstone and rudstone	Base conformable with Cona and Esmisek Fms unconformable on the ophiolitic complex. Angular unconformity with K1c1 and Gökdere Fms. Faulted contacts with other formations numerous.	> 400m

1013 Table 1. Summary of the characteristics of the lithostratigraphic units discussed in the text.

	Serinyo	Kan1	Kan2	Kan3	Gok 1	Gok 2	Gok 3	Gok 4
	1							
Serpentinite	0	0	27	10	95	80	33	40
Chert	14	9	12	2	0	0	3	2
Algal lmst	73	0	0	0	0	0	0	0
Chert + lmst	13	20	26	21	0	0	0	0
Bioclastic lmst	0	5	12	13	0	0	0	0
Nummul. lmst	0	0	0	0	0	0	4	1
Undiff lmst	0	74	42	35	5	20	5	0
Total	100	108	119	81	100	100	45	43

1014

1015 Table 2. Clast counts from conglomerate horizons at Serinyol (Ser), Kanlidere (Kan) and Gökdere  
1016 (Gok), location of sites shown on figures 6 and 9. The clast count was undertaken by drawing a 1x1  
1017 m grid upon the outcrop, 10 cm intersections were marked and the clast at each intersection  
1018 counted, giving the clast composition of ~ 100 clasts at each location.

Sample No	SB73A	SB71A	SB77A	SB94A	SB142A
Age	L.Mio	L. Mio	L. Mio	U.Mio	U. Mio
S.Calcite	20	31	37.5	28.5	19.5
Micrite	2	1.5	10.5	6.5	7
Qtz(m)	1	7.5	0	10.5	5.5
Qtz(p)	1.5	6.5	0	10	11.5
Ophiolite	51.5	7	48.5	13.5	11.5
bioclast	0	0	1	2	0
mica	0	0.5	0	2	0
carbonate	5.5	19	1.5	12.5	30
siliciclastic	14.5	17	0.5	8	6
feldspar	0	1	0	4	0.5
opaque	4	4	0	2.5	2
other	0	5	0.5	0	6.5
Total	100	100	100	100	100

1019

1020 Table 3. Point-counting results for sandstones. Two hundred points were counted for each thin-  
1021 section in order to have a statistically meaningful sample group. For locations of samples (SB73A,  
1022 etc.) see Fig. 1. S.Calcite = sparry calcite; Qtz (m) = monocrystalline quartz; Qtz (p) =  
1023 polycrystalline quartz.

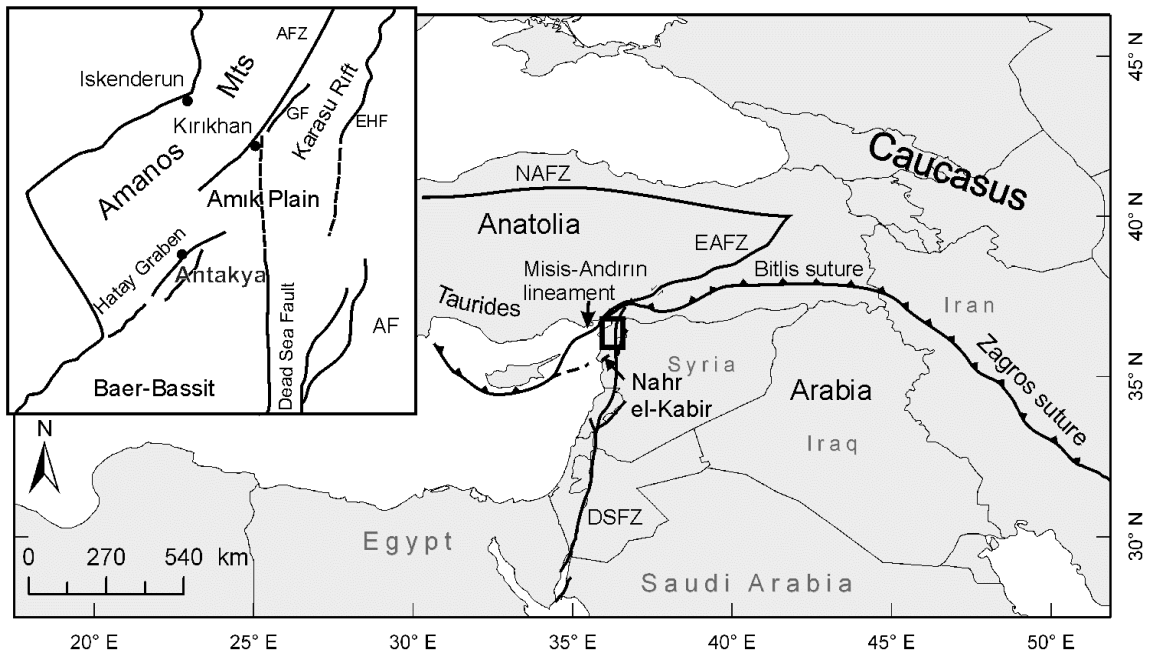
Sample	Age	Fm.	Quartz	Calcite	Smectite	Clinochrysoile	Albite	Dolomite	Muscovite	Others	Total
SB72A	U.Mio	G	29	51	0	0	12	2	0	6	100
SB95A	U.Mio	G	28	49	0	0	0	2	5	16	100
SB98A	U.Mio	G	14	57	0	8	2	0	16	3	100
SB140A	U.Mio	G	15	56	0.1	22	5	0	0	1.9	100
SB135A	U.Mio	G	38	59	0	3	0	0	0	0	100
SB137A	U.Mio	G	26	57	0	0	10	0	6	1	100
SB104A	L.Mio	K	32	41	0	0	10	0	0	17	100
SB76A	L.Mio	K	20	5	16	39	0	0	20	0	100
SB126A	Eocene	H	17	61	0	1	0	0	14	7	100
SB128A	Eocene	H	20	78	0	0	2	0	0	0	100
SB133A	Eocene	H	19	79	0	0	2	0	0	0	100

1024

1025 Table 4. XRD determinations of fine-grained sediments (sample locations shown on Fig. 1). Two  
1026 samples were analysed from the K1c1 Formation (SB76A & SB104A), both have compositions rich  
1027 quartz and clinochrysoile. Sample SB76A contains abundant smectite (16%) and muscovite (20%)  
1028 but low calcite (5%). Sample SB104A, by comparison, has no smectite or muscovite but has a high  
1029 (56%) calcite content. Six samples were analysed from the Gökdere Formation. All have  
1030 significant amounts of quartz (14-38%) and high calcite (31-78%) contents. Albite and muscovite  
1031 also are relatively abundant. Formation codes; G = Gökdere; K = K1c1 and H = Hacıdağ.

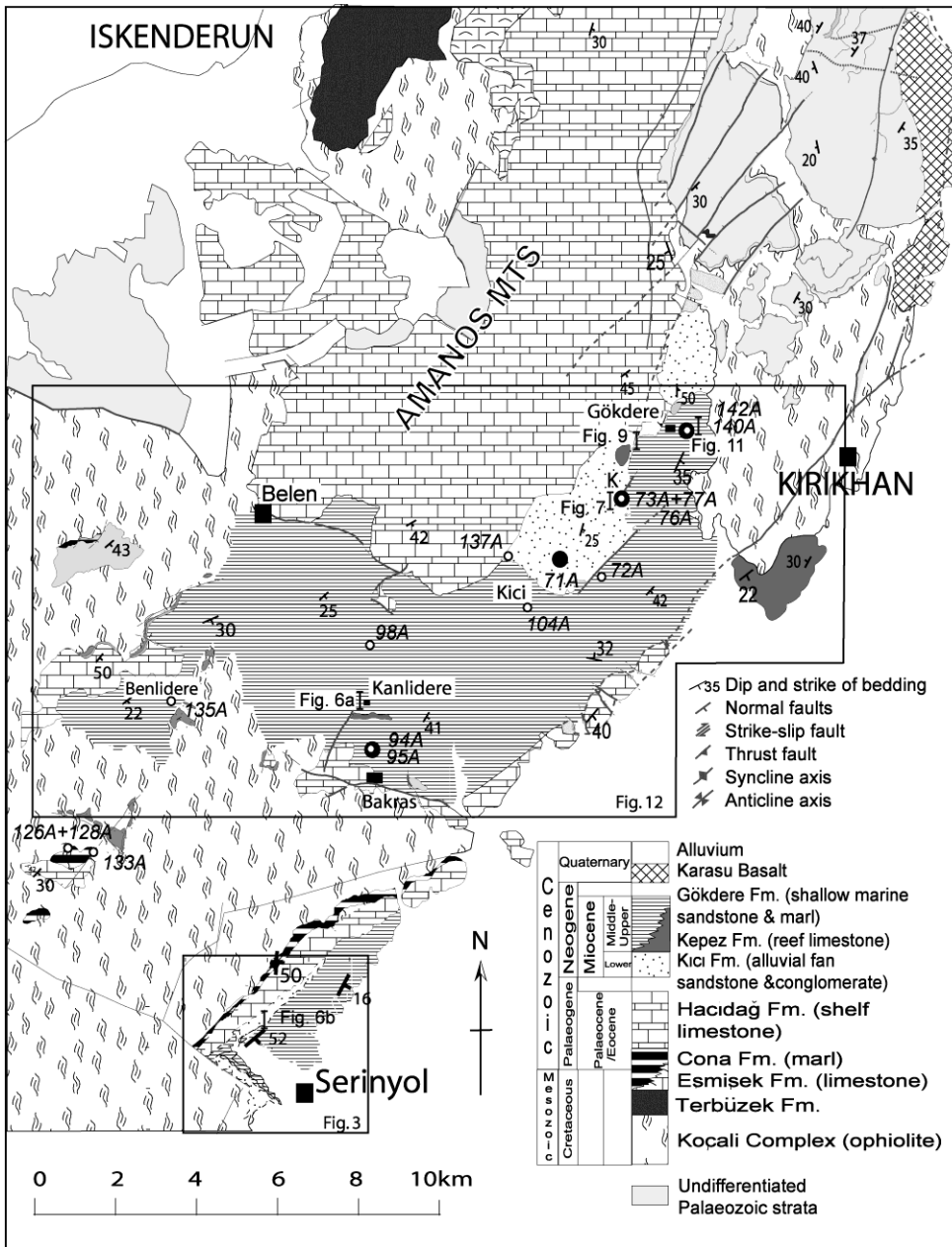
1032

1033 **Figures**



1034

1035 Figure 1. Regional geodynamic framework, small box shows location of the study area. Inset box  
 1036 shows major faults of the study area and locale, DSFZ: Dead Sea Fault Zone; EAFZ, East Anatolian  
 1037 Fault Zone; NAFZ, North Anatolian Fault Zone; AFZ, Amanos Fault Zone, EHF, East Hatay Fault;  
 1038 AF, Afrin Fault; GF, Guzelce Fault.



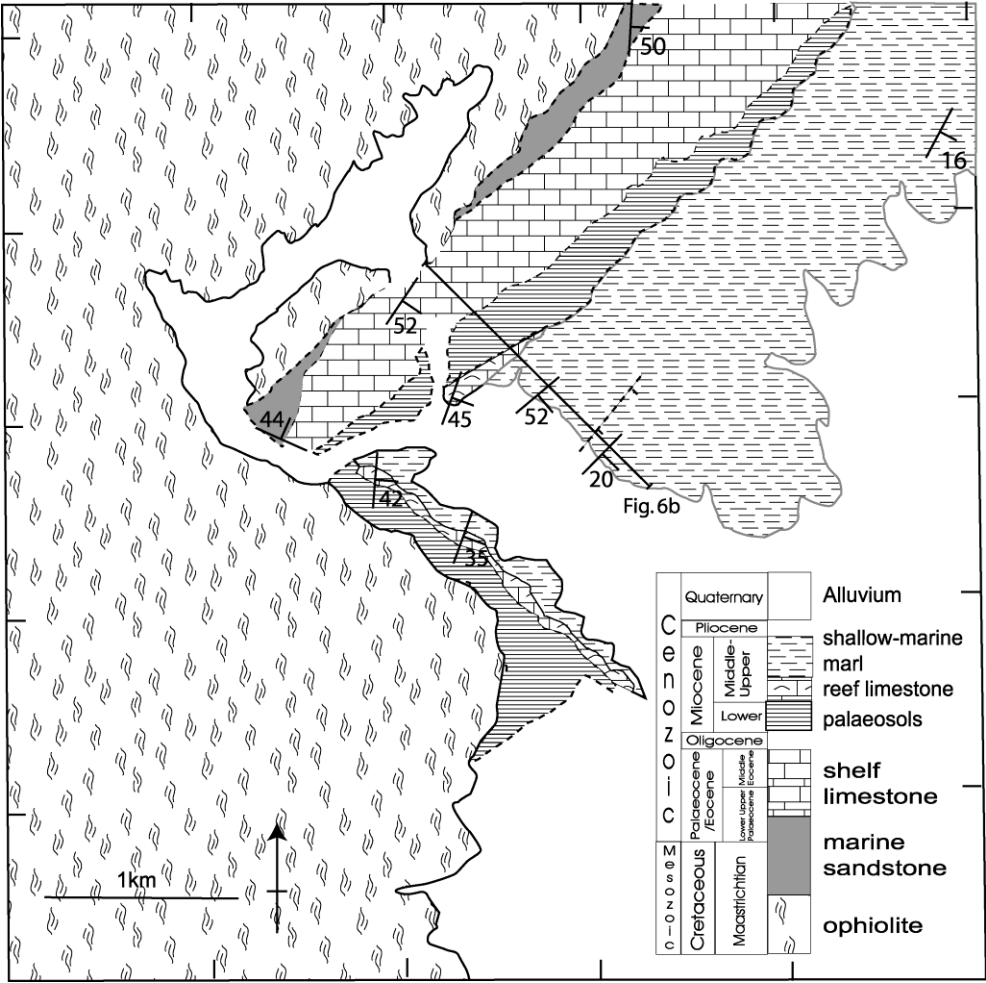
1039

1040

1041 Figure 2. Geological map of the northern part of the study area around the towns of Kırıkhan and  
 1042 Belen, showing the main places discussed in the text and the locations of samples used in  
 1043 petrological analysis (modified from Boulton et al., 2007); black circles indicate locations where  
 1044 sandstones for point-counting were collected, white circles indicate locations where fine-grained  
 1045 sediments were taken for XRD analysis, bars with appended Figure numbers indicate locations of  
 1046 logs, while boxes indicate the extent of figures 3 and 13. The letter K indicates the location of the  
 1047 type section of the Kıcı Formation at Kurtisoğuksu.

1048

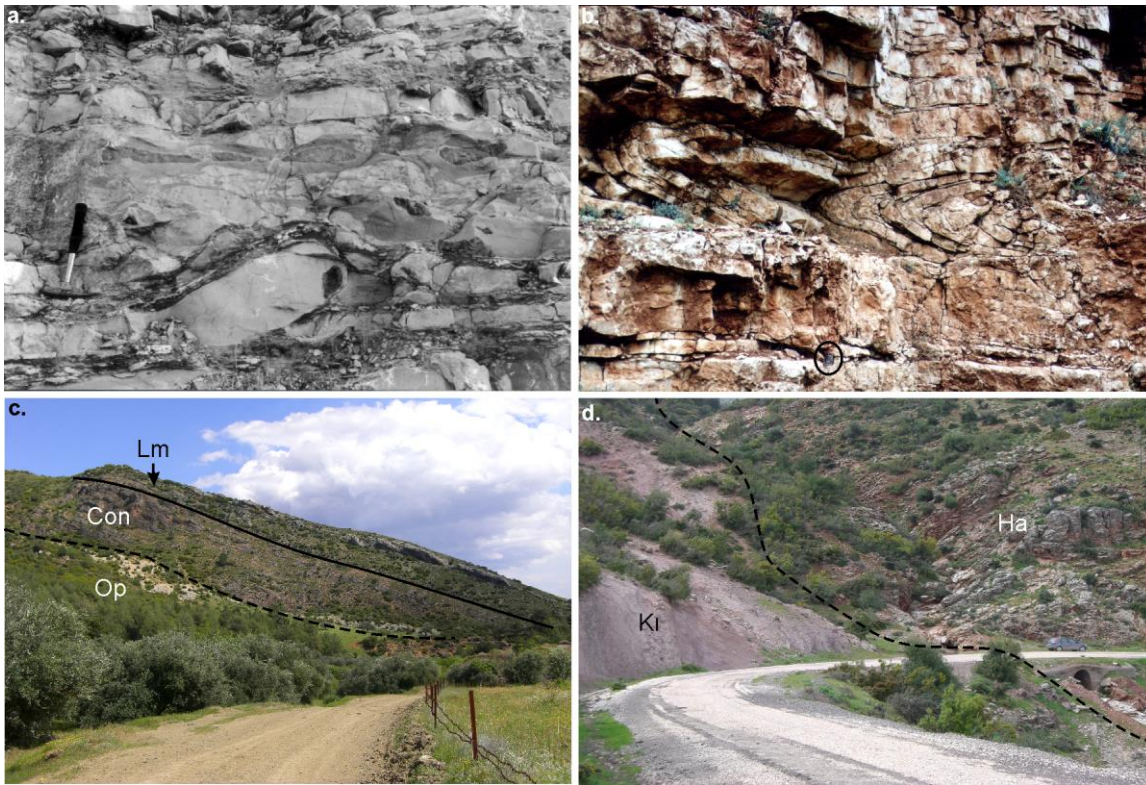
1049



1050

1051

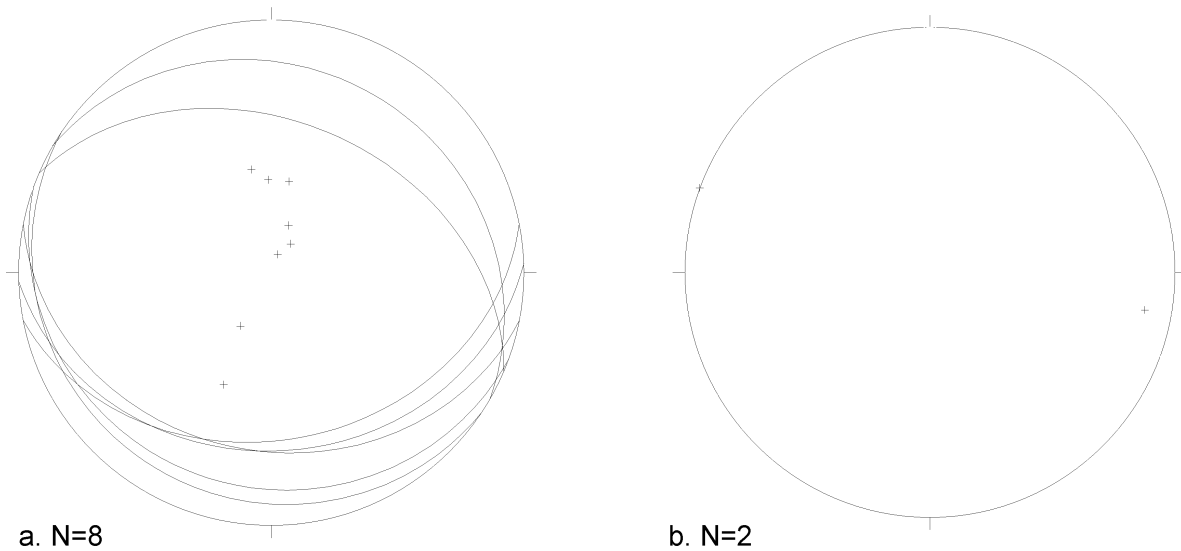
1052 Figure 3. Geological map of the area around Serinyol, see figure 2 for the location within the  
 1053 Karasu Rift. Black line indicates the location of the log shown in figure 6b. Note the town of  
 1054 Serinyol is located under the key.



1055

1056 Figure 4a. Incipient slump in thin-bedded Eocene limestone at 0255391/4036316 (Map sheet  
 1057 Antakya P36-a2), north of the Kırıkhan-Antakya road; b). Isoclinal recumbent slump fold observed  
 1058 in Eocene limestones (circled compass-clinometer provides scale) just off the main Belen road at  
 1059 grid ref. 0252481/4041026 (Map sheet Antakya P36-a2). Orientations of this fold hinge and the  
 1060 incipient slump shown in (a) demonstrate that the palaeoslope was inclined to the north (see fig. 5 for  
 1061 bedding data); c). General view of the Eocene sediments near Serinyol at 0248123/4029755 (Map  
 1062 sheet Antakya P36-a3). Three units can be observed the basal unit is ophiolite (Op), an erosive  
 1063 unconformity separates the basement from the overlying Eocene composed of a basal conglomerate  
 1064 (Con) and upper bedded limestones (Lm) above; d). View of the Eocene (Ha - RHS) – Lower  
 1065 Miocene (K1 - LHS) boundary near the village of Gökdere, along which a stream has flowed.  
 1066 Eocene limestones are folded, while the overlying K1c1 formation is unfolded, dipping  
 1067 southeastwards (towards the camera). The Lower Miocene strata is formed of a basal algal  
 1068 boundstone representing a brief marine incursion, with continental clastics above.

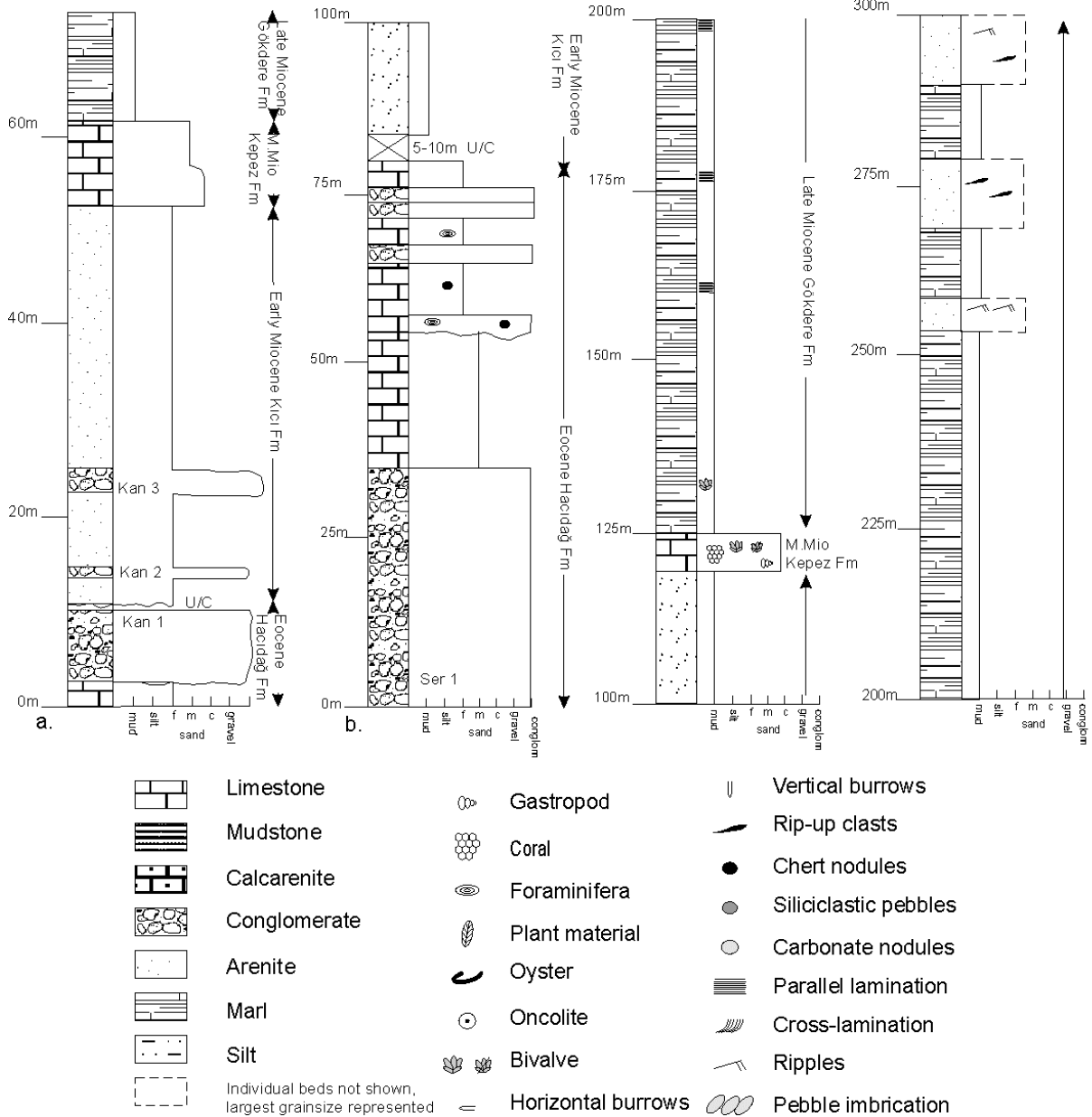
1069



1070  
 1071 Figure 5a). Bedding plane data (shown as great circles and pole to plane - the crosses) for limbs of  
 1072 slump folds observed in the Eocene Hacıdağ Formation; b). Crosses indicate orientation of hinge  
 1073 lines of measured slump folds (Fig. 4b). Both sets of data indicate the general orientation of the  
 1074 palaeoslope was N to NNE; perpendicular to the hinges of the folds that form parallel to the strike  
 1075 of the palaeoslope.



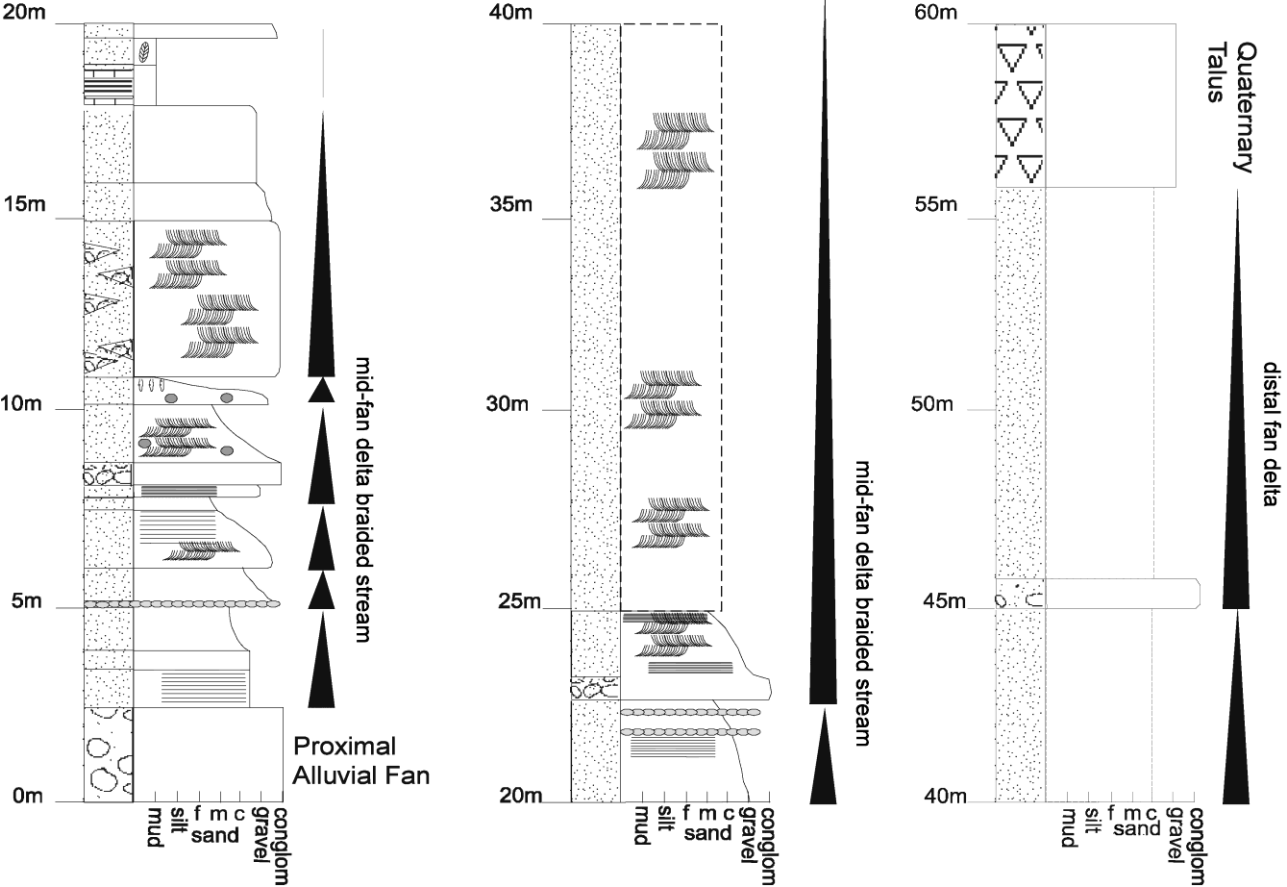
1076



1077

1078 Figure 6a). Log of Sediments at Kanlidere (on figure 2). Kan1, 2, 3 and Ser 1 show the positions  
 1079 where conglomerate clast counts were undertaken, see Table 2 for results; b. Log of sediments at  
 1080 Serinyol (see figure 3 for position of logged section). Key for all logs shown at the bottom.

1081



1082

1083

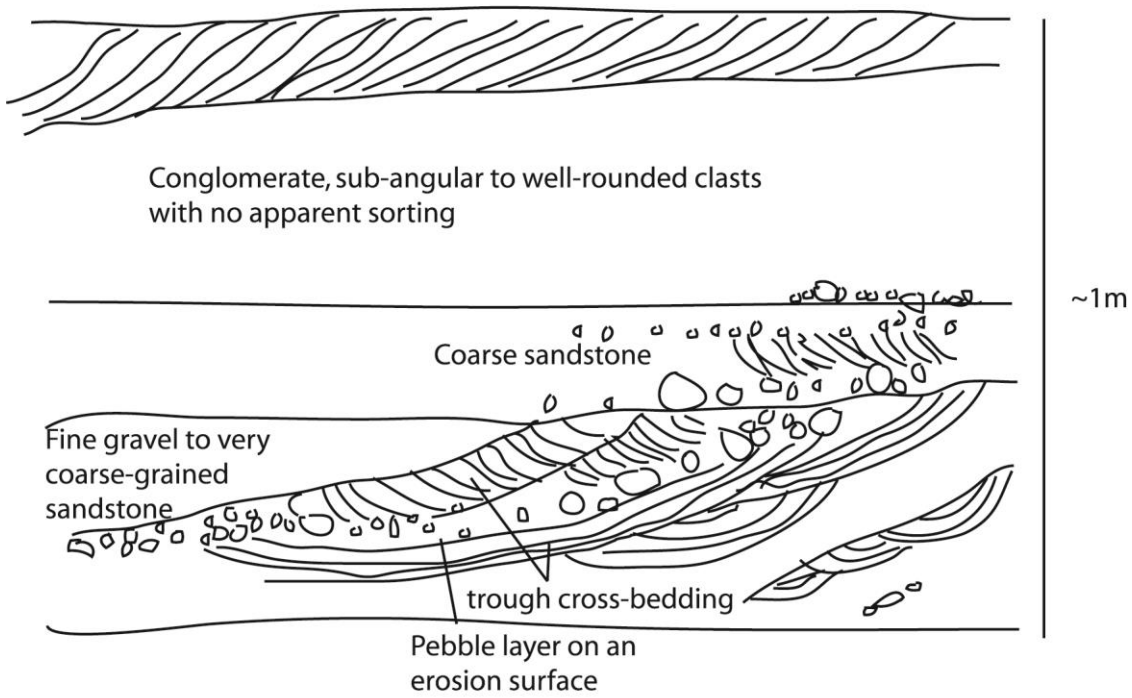
1084 Figure 7. Log of K1c1 formation at the type section (K; Fig. 2) with sedimentary environments and  
 1085 fining-upwards cycles shown. Fining-upwards sequences may represent bar processes or where a  
 1086 basal conglomerate is present, may be a channel fill deposit (modified from Boulton et al., 2007).

1087 See figure 6 for key.



NW

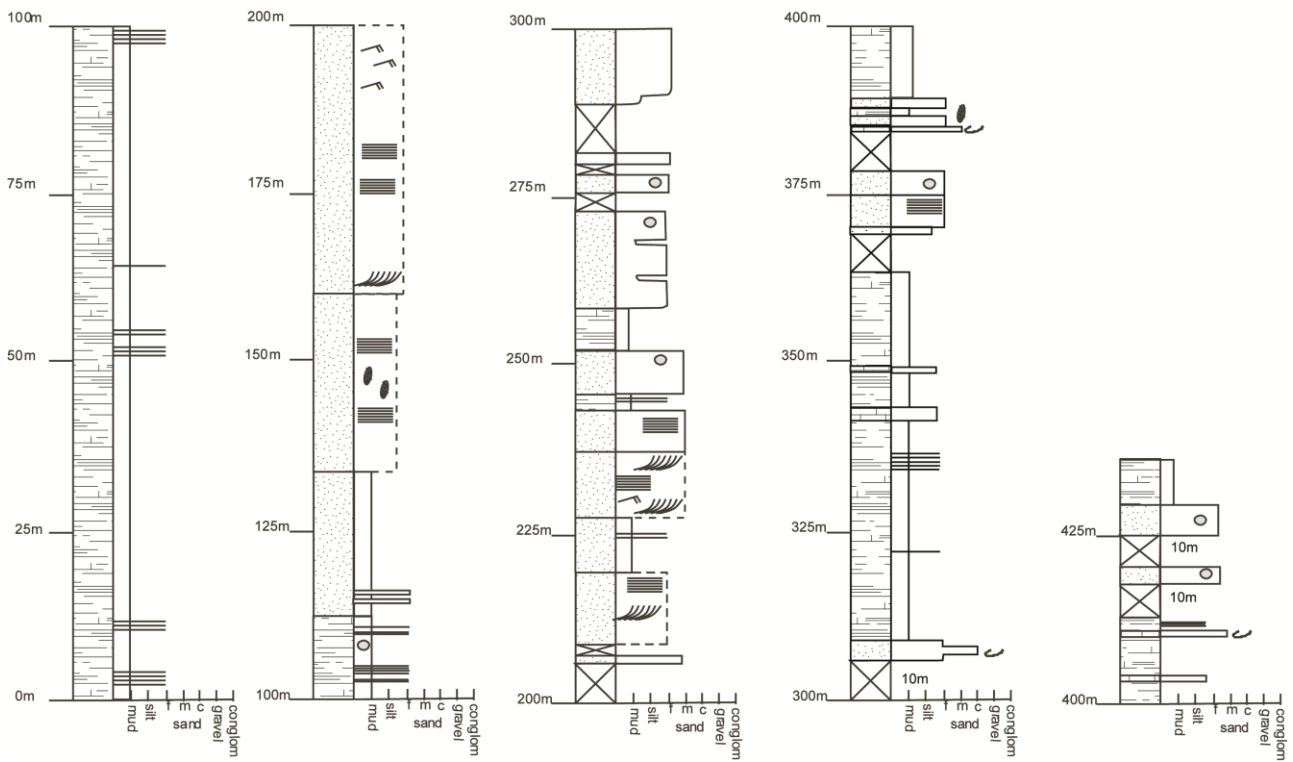
SE



1088

1089 Figure 8. Field photograph and sketch of cross-bedded sandstones typical of the K<sub>1c1</sub> Formation,

1090 from the type section (K; Fig. 2). See figure 6 for key.



1091

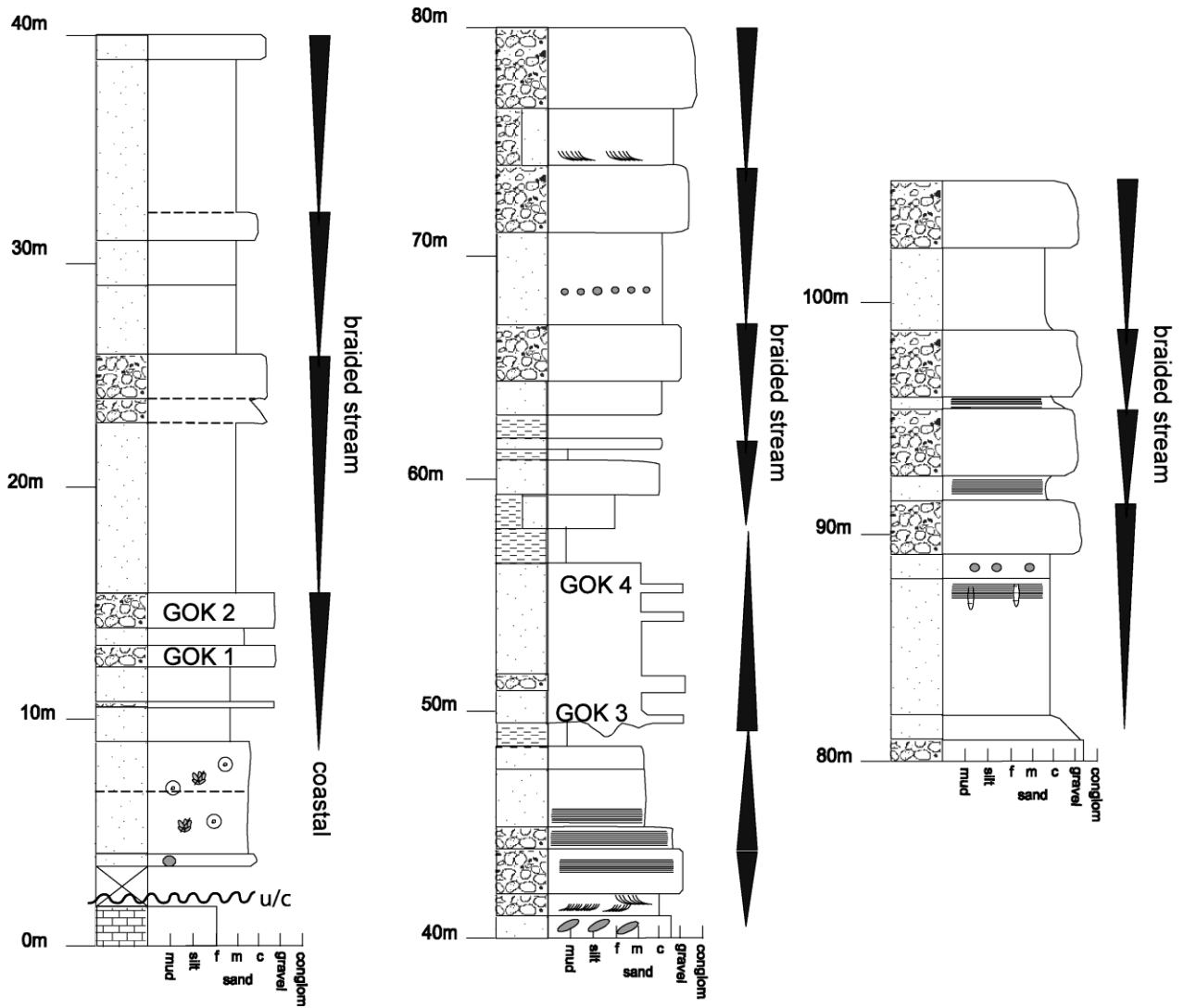
1092 Figure 9. Log of the Kıcı Formation near the village of Gökdere (Fig. 2), the sequence is interpreted  
 1093 as an alluvial fan deposit where coarsening-upwards cycles possibly represent progradation of  
 1094 individual fan lobes. Gok 1, 2, 3, 4 refer to locations where conglomerate clast counts were  
 1095 undertaken, results shown in table 2.





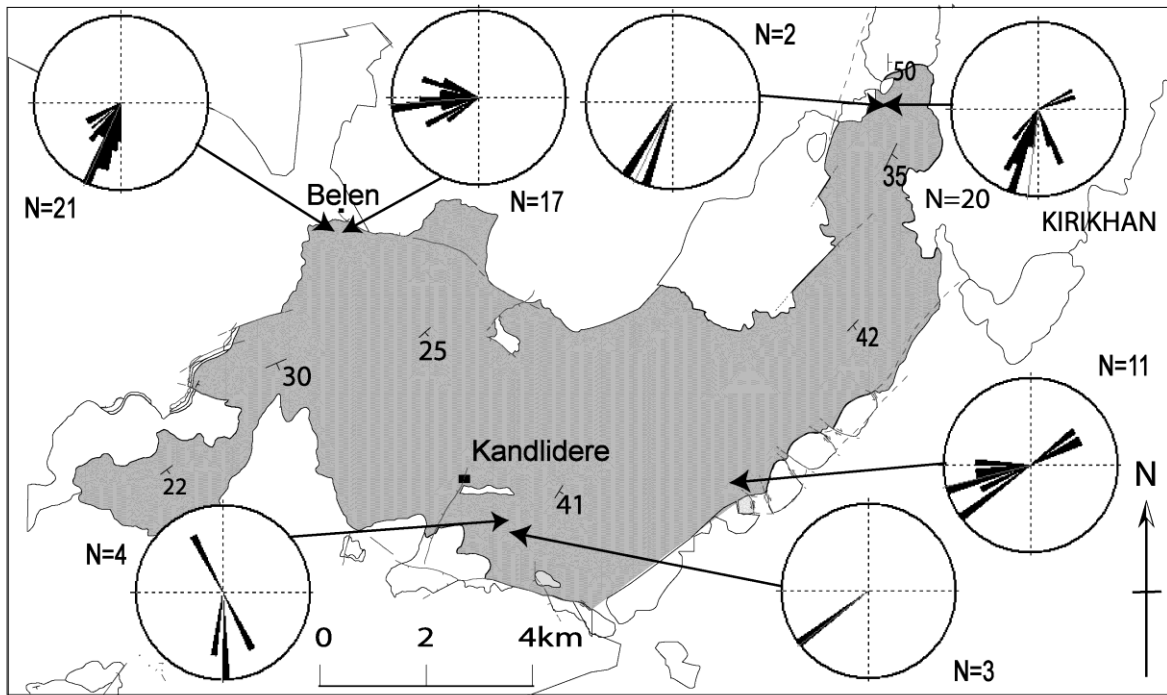
1096

1097 Figure 10a. Close up of a conglomerate horizon in the K1c1 Formation, at Kanlidere, note borings in  
 1098 limestone clasts; b). Close-up of blocks of coralline limestone from the Kepez Formation observed  
 1099 near Serinyol; c). View over the village of Gökdere with part of Cenozoic sedimentary sequence  
 1100 exposed from left to right in the foreground. In the lower left the ophiolite complex (Op) is  
 1101 observed, above is the Upper Miocene Gökdere Formation (Go) dipping southeastwards (to the  
 1102 right). The Middle Miocene Kepez Formation (Ke) can be observed as a laterally discontinuous  
 1103 outcrop exposed in the side of hill (in the centre of the field of view), the K1c1 Formation is not  
 1104 present at this location; d). View of the middle of the Gökdere Formation at the type section  
 1105 showing a typical sand-body on the left hand side.



1106

1107 Figure 11. Log of the Gökdere Formation at Gökdere (Fig. 2). See figure 6 for key. The sequence is  
 1108 interpreted as a regressive shallow-marine sequence.



1109

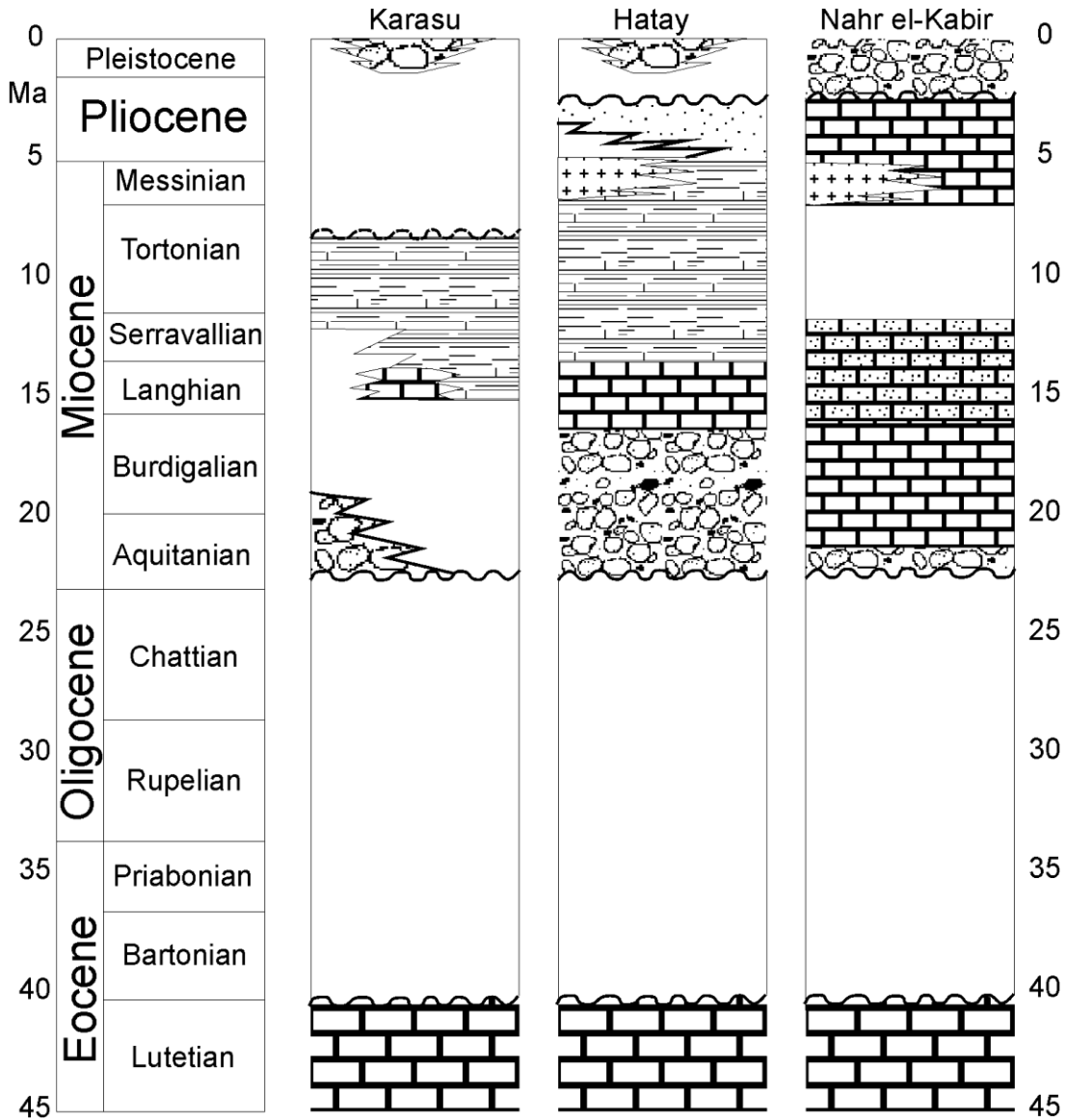
1110 Figure 12. Rose diagrams of measured palaeocurrents from the Upper Miocene Gökdere Formation

1111 in the central part of the study area (extent of this map shown on figure 2). N = No. of measurements

1112 at each locality.

1113

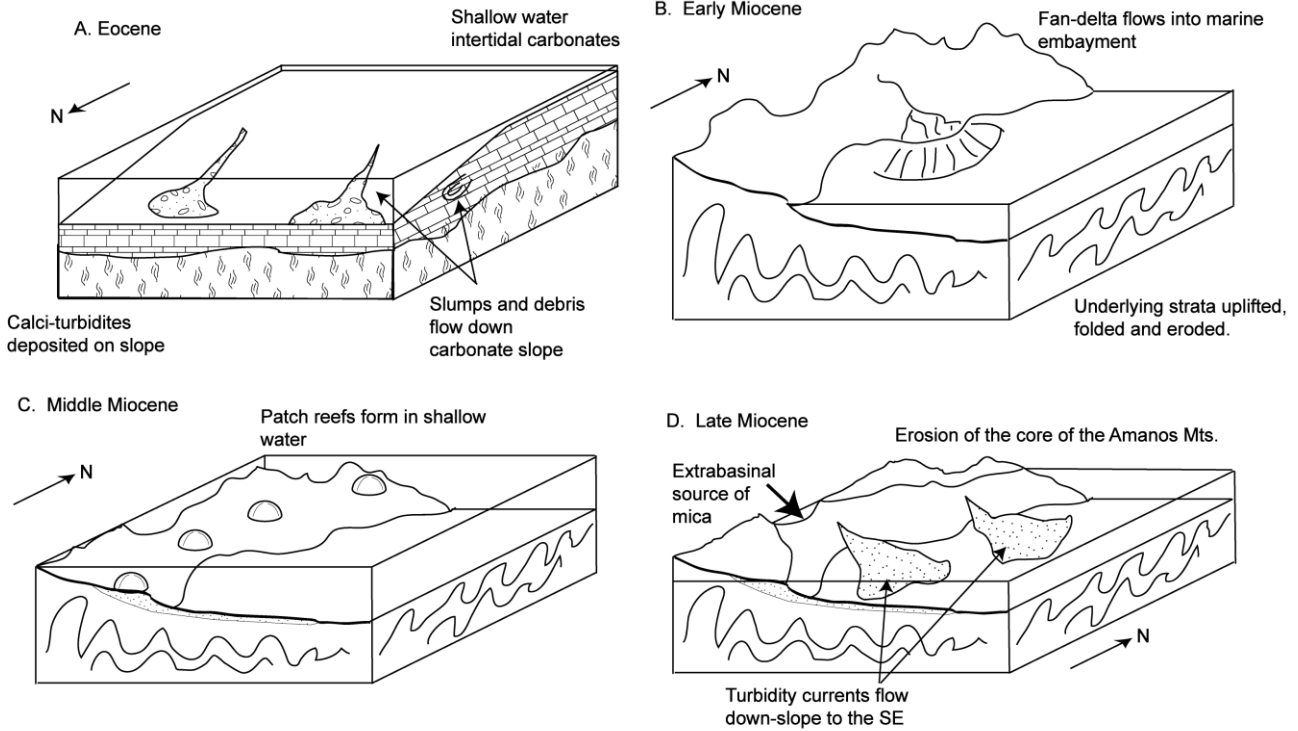
1114



1115

1116 Figure 13. Stratigraphic columns showing the stratigraphy of the Karasu Rift, Hatay Graben and  
 1117 Nahr el-Kabir Graben (locations of areas shown on Figure 1). Note the similarities between the  
 1118 Karasu Rift and adjacent Hatay Graben and the differences of both areas to the Nahr el-Kabir  
 1119 Graben to the south. See figure 6 for key.





1120

1121 Figure 14. Block diagrams illustrating inferred palaeogeographical conditions during A) Eocene; B)

1122 Lower Miocene; C) Middle Miocene; D) Upper Miocene and E) Pliocene to Recent times. N.B.

1123 Note the reversed orientation of diagram (A).

1124

1125

1126

1127

1128

1129

1130